New Jersey Institute of Technology
Digital Commons @ NJIT

Dissertations   Theses and Dissertations

Spring 2018

Borehole communication via drill strings in oil wells

Ali Hamdan Alenezi
New Jersey Institute of Technology

Follow this and additional works at: https://digitalcommons.njit.edu/dissertations

Part of the Electrical and Electronics Commons

ABSTRACT

BOREHOLE COMMUNICATION VIA DRILL STRINGS IN OIL WELLS

by
Ali Hamdan Alenezi

The performance of multichannel and single channel accelerometers used as uphole communication receivers is studied. Using measured channels from the drill string testbed, it is shown that one tri-axial accelerometer can provide nearly uncorrelated signals when compared to two single channel accelerometers. Having uncorrelated signals at the uphole receiver provides a diversity which in turn can lead to an increase in the communication system performance. The use of a strain sensor as a receiver in borehole communication is proposed. Using measured channels from the drill string testbed, the performance of a strain receiver with a single-accelerometer receiver is compared. The results show that the strain receiver has better performance than the single accelerometer receiver, and is further demonstrated that the strain channel impulse response has a better structure than a single-accelerometer channel impulse response. Furthermore, the multichannel reception using several receivers with the aim of improving communication system performance is studied. The combination of a strain sensor and a tri-axial accelerometer as a four-channel receiver is proposed. Given the complexity of studying the strain channel and the three acceleration channels analytically, experiments are conducted to obtain these channel impulse responses. The channel measurements show that these wireless channels are nearly uncorrelated and therefore can provide a diversity gain. This is further confirmed by the low bit error rates that this system provides. Comparison with single channel receivers shows the usefulness of the proposed system for wireless communication via drill strings.

BOREHOLE COMMUNICATION VIA DRILL STRINGS IN OIL WELLS

by
Ali Hamdan Alenezi

A Dissertation
Submitted to the Faculty of
New Jersey Institute of Technology
In Partial Fulfillment of Requirements for the Degree of
Doctor of Philosophy in Electrical Engineering

Helen and John C. Hartmann Department of
Electrical and Computer Engineering

May 2018

APPROVAL PAGE

BOREHOLE COMMUNICATION VIA DRILL STRINGS IN OIL WELLS

Ali Alenezi

Dr. Ali Abdi, Dissertation Advisor	Date
Professor of Electrical and Computer Engineering, NJIT	

Dr. Alexander M. Haimovich, Committee Member	Date
Professor of Electrical and Computer Engineering, NJIT	

Dr. Joerg Kliewer, Committee Member	Date
Associate Professor of Electrical and Computer Engineering, NJIT	

Dr. Osvaldo Simeone, Committee Member	Date
Professor of Electrical and Computer Engineering, NJIT	

Dr. Eliza Michalopoulou, Committee Member	Date
Professor of Mathematics, NJIT	

BIOGRAPHICAL SKETCH

Author: Ali Hamdan Alenezi

Degree: Doctor of Philosophy

Date: May 2018

Undergraduate and Graduate Education:

- Doctor of Philosophy in Electrical Engineering,
  New Jersey Institute of Technology, Newark, NJ, 2018

- Master of Science in Electrical Engineering,
  Royal Institute of Technology(KTH), Stockholm, Sweden, 2011

- Bachelor of Science in Electrical Engineering,
  King Saud University, Riyadh, Saudi Arabia, 2007

Major: Electrical Engineering

Presentation and Publications:

A. Alenezi and A. Abdi, "On multiple wireless channels in oil wells drill strings," IEEE Wireless Commun. Lett., vol. 6, pp. 738-741, 2017.

A. Alenezi and A. Abdi, "Experimental results on acoustic communication thru drill strings using a strain sensor receiver," *in Proc. Meetings on Acoustic (173rd Meeting of the Acoustical Society of America)*, Boston, MA, 2017.

A. Alenezi and A. Abdi, "A comparative study of multichannel and single channel accelerometer sensors for communication in oil wells," *in Proc. in IEEE International Conference on Communication and Signal Processing*, Melmaruvathur, India, 2017.

To my wonderful family, Omar, Hana, and Huda.

ACKNOWLEDGMENT

First, I would like to thank my advisor Professor Ali Abdi, for his guidance, time, encouragement, continuous support, and help. I would like also to thank my committee members, Professor Alexander M. Haimovich, Professor Eliza Michalopoulou, Professor Joerg Kliewer, and Professor Osvaldo Simeone for their comments and suggestions.

Further thanks go to all the professors who have taught me throughout my graduate study. I also thank all of the staff at the Department of Electrical and Computer Engineering and the Office of Graduate Studies at the New Jersey Institute of Technology.

I am grateful for the support and good wishes I always received from my colleagues and friends. Finally, I would like to deeply thank my family for their support, prayers, and patience

TABLE OF CONTENTS

LIST OF TABLES

LIST OF FIGURES

CHAPTER 1

INTRODUCTION

1.1 Background

Hydrocarbon resources such as oil and gas are located several thousands of feet underground. Current civilization relies mainly on these hydrocarbon resources for the generation of electricity, transportation, and in the manufacture of numerous products. To extract the oil and gas one need to drill deep wells that go several thousands of feet underground with, during the drilling process, the drill bit penetrating different earth layers, as shown in Figure 1.1.

The earth layers that are penetrated by the drill bit have different characteristics, and from these characteristics, the oil engineer can predict the proximity of hydrocarbon reservoirs as well as their types. Usually, there are several sensors placed close to drill bit to collect information such as temperature, humidity, pressure, resistivity, radiation, etc. The process of sending this information from downhole to the surface is called "telemetry". If the information is sent during the process of drilling, it is called Logging While Drilling (LWD) because it is real-time communication, however, in cases where the drilling process is stopped to send the information to the surface, it is then called off-line telemetry. There are different telemetry methods that can be used to send information from downhole to the surface, including mud pulse telemetry, electromagnetic waves, wireline telemetry, and acoustic telemetry. During the drilling operation, there is a special kind of mud pumped through the drill string, the main role of which is to carry the cuttings of crushed formation from downhole to the surface through the hollow space between the drill string and the wall of the well. This mud is exploited to send the information that is collected by the

sensors to the surface by modulating it using a valve that controls the mud flow [1,2], as

shown in Figure 1.2.
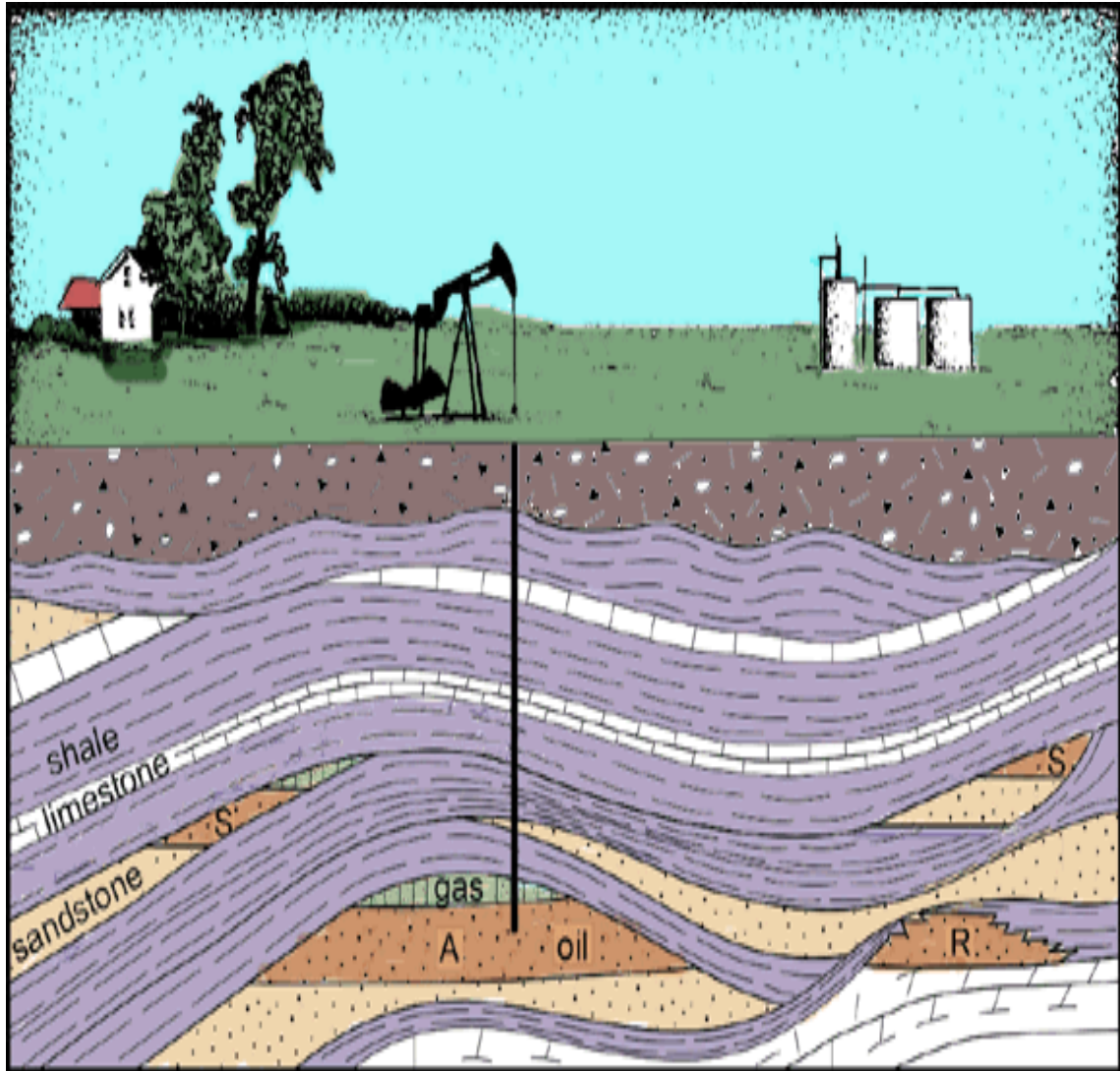
Figure 1.1 Oil and gas reservoirs underground.
Source: Hydrocarbons deposits. Reprinted from school of geosciences in University of Sydney, by P. Huston, retrieved April 12, 2017, from http://www.geosci.usyd.edu.au/users/prey/ACSGT/EReports/eR.2003/GroupD/Report2/web%20pages/hydrocarbon_deposits.html.
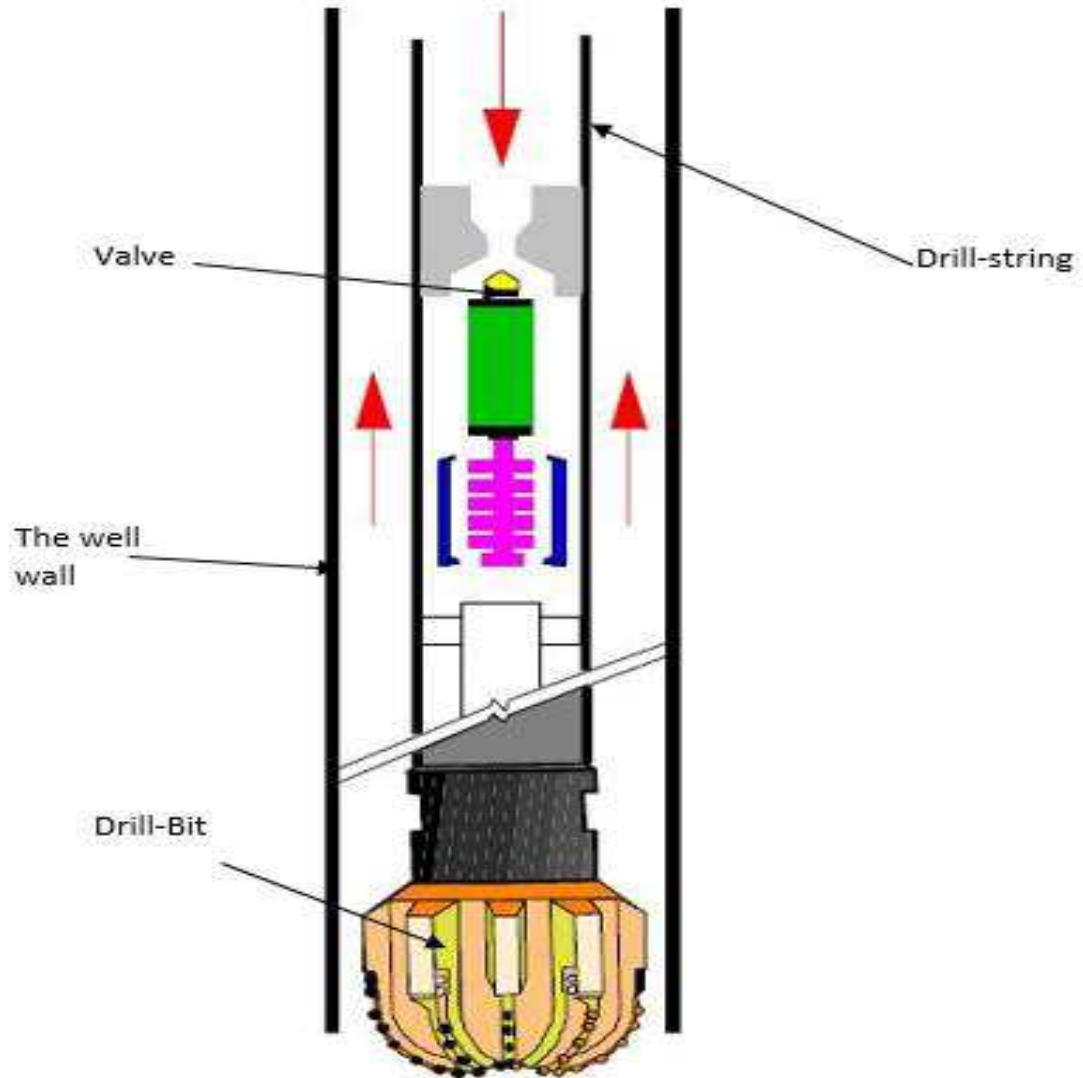
Figure 1.2 Mud-pulse telemetry.
Source: Mud pulse telemetry. Reprinted from Measurement While Drilling (MWD) and its Application in Directional Drilling in directional drilling technology website, Retrieved October 23, 2015, from http://directionaldrilling.blogspot.com/2011/07/21-measurement-while-drilling-mwd-and.html.

Mud-pulse telemetry is real-time telemetry and does not interfere with the drilling operation; however, its data rate is very low at, in typical circumstances, 2-3 bits per second. The mud-pulse telemetry is the only commercial telemetry used in real-time communication during well drilling. Electromagnetic waves can offer a large bandwidth [3,4] although in borehole communication these are highly attenuated due to the formation

resistivity profile. Wireline telemetry is a form of off-line telemetry, where the driller needs to take the entire drill-string out of the well, and then load a pipe that contains multiple sensors using long cables. This pipe is connected with coaxial cable to establish a communication link from downhole to surface and this form of telemetry interferes with the drilling operation and has very high cost, including that associated with the time delay in the well drilling. Acoustic telemetry is a promising technique, which uses the drill string as a channel medium to send information. As such it does not interfere with the drilling operation and it offers a high data rate at several hundreds of bit per seconds. However, as a drill string is constructed from a series of pipes connected via tool joints, and due to mismatch between the pipes and tool joints, there are many forward and backward reflections of a transmitted acoustic signal, which result in a complex multipath channel.

The idea of using acoustic waves for oil well communication through the drill string was first proposed by the Sun Oil Company in 1948 and they conducted field test experiments to measure the attenuation of acoustic waves that propagated through the drill string [5]. After that, several studies were performed on drill strings to discover the drill string channel characteristics [6,7,8]. The studies of the acoustic drill string channel characteristics concluded that, since the acoustic wave propagate in an inhomogeneous channel that has a periodic structure, the drill string channel impulse response is characterized by heavy reflections, as shown in Figure 1.3. On the other hand, the channel frequency response has periodic pass-bands and stop bands forming a comb-filtering-like pattern, also in Figure 1.3.
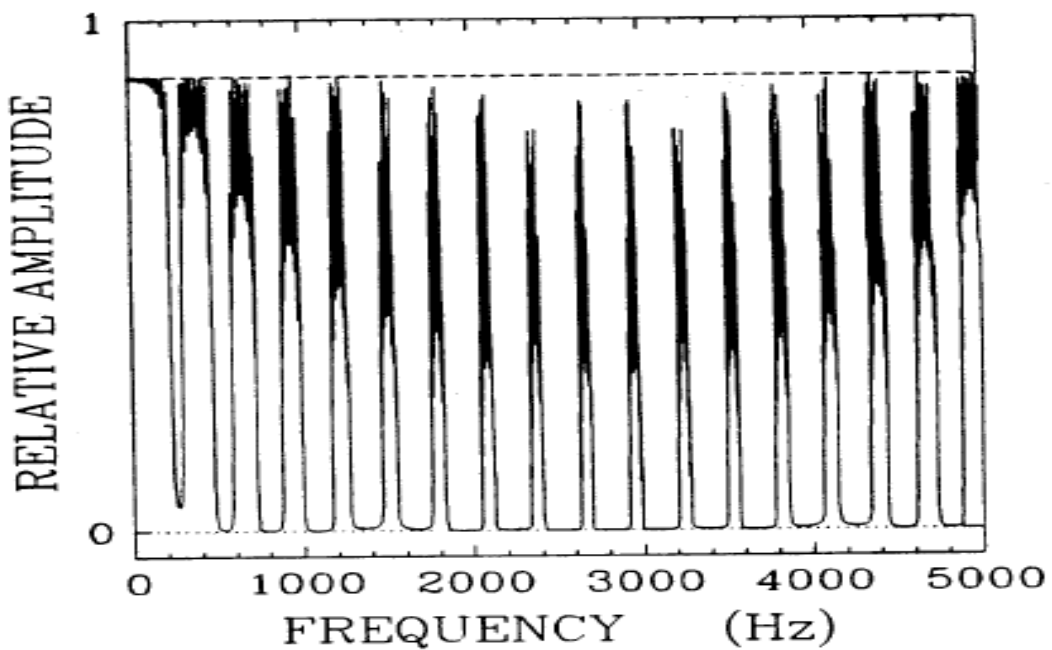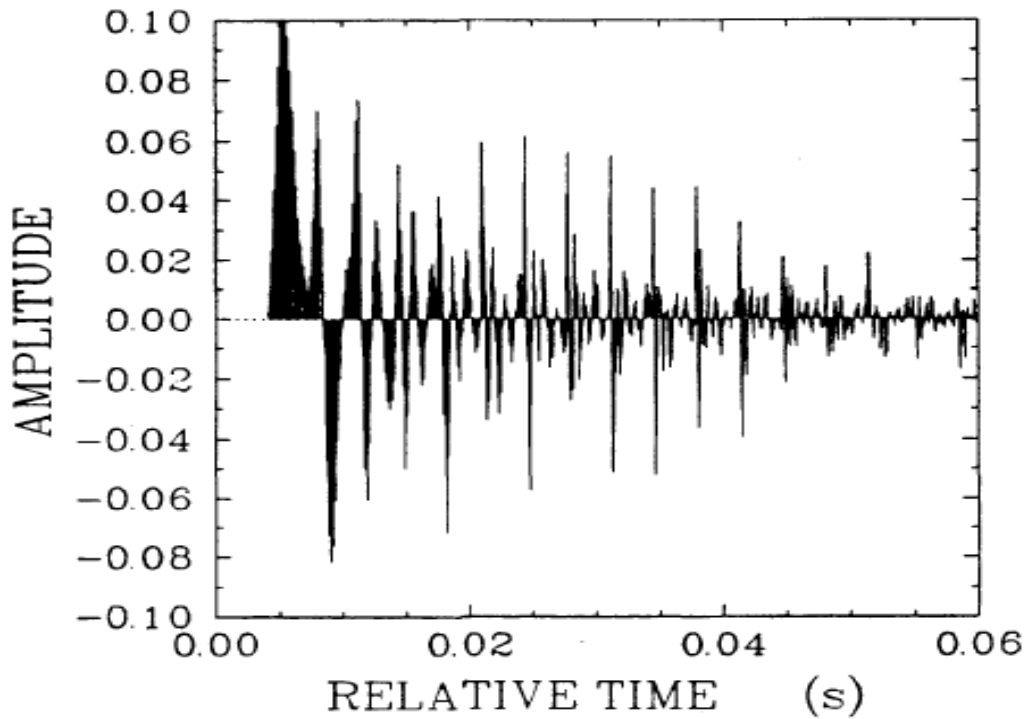
Figure 1.3 Drill string channel impulse and frequency responses generated from a channel model.
Source: Drill string Channel impulse and frequency responses. Reprinted from [7].

Based on the drill string channel structure, the use of an acoustic Orthogonal Frequency Division Multiplexing (OFDM) transmission scheme has been proposed in [9]. Different machines used around the well produce in-band high intensity noise, and by exploiting the upward and downward propagation modes of the acoustic wave through the drill string, a two-receiver noise cancelation method has been proposed in [10] to reduce the background noise effect during borehole communication.
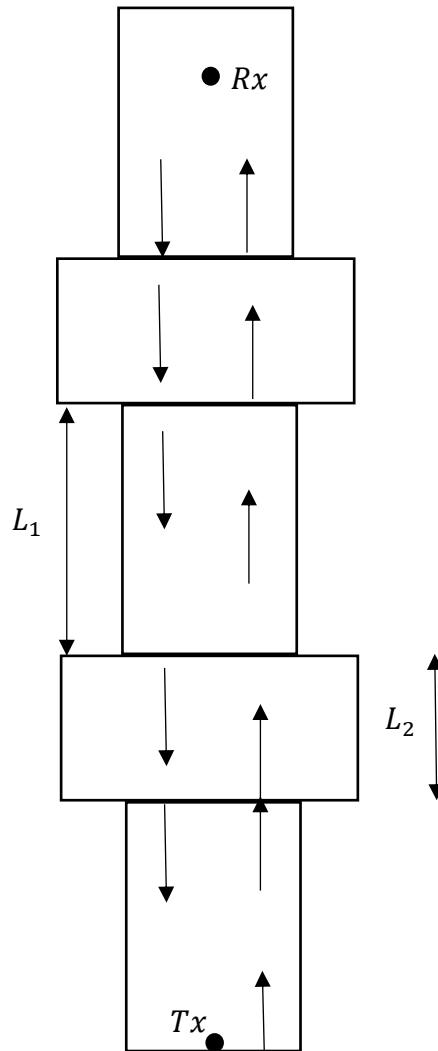
Figure 1.4 Up-going down-going wave propagation through drill string.

1.2 Pipe String Channel Model Using Wave Propagation Theory

In wireless communication systems, the most important part over which we cannot have control, is the channel, which mainly determines the data capacity that we can convey from the transmitter to the receiver. The drill string consists of pipes that are connected with each other using threaded joints, as shown in Figure 1.4. The acoustic waves propagated through the drill string encounter scattering and attenuation due to the mismatch of impedance between the pipes and the tool joints, which results in heavy reflections at the receiver side. There are two kinds of waves that propagate
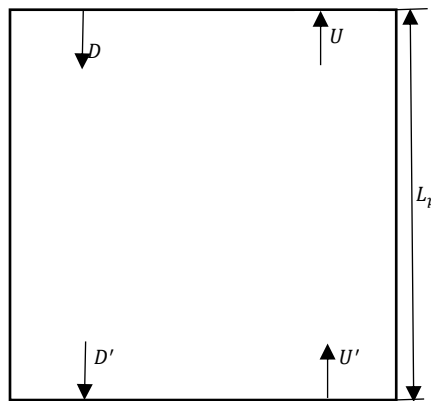
Figure 1.5 Acoustic wave propagation through one pipe.

through the drill string, up-going waves and down-going waves, as shown in Figure 1.4. Wave propagation theory can be used to model the acoustic wave propagation through different layers, and this method can be employed to model the drill string channel [11]. We can describe the wave propagation through the pipe shown in Figure 1.5 using the following matrix relation

$$\begin{bmatrix} U \\ D \end{bmatrix} = \begin{bmatrix} e^{j\omega T_p} & 0 \\ 0 & e^{-j\omega T_p} \end{bmatrix} \begin{bmatrix} U' \\ D' \end{bmatrix} \tag{1.1}$$

where

$$M_p = \begin{bmatrix} e^{j\omega T_p} & 0 \\ 0 & e^{-j\omega T_p} \end{bmatrix} \tag{1.2}$$

represents the wave propagation between the pipe ends and the following matrix represents the acoustic wave propagation between the tool joint ends

$$M_j = \begin{bmatrix} e^{j\omega T_j} & 0 \\ 0 & e^{-j\omega T_j} \end{bmatrix} \tag{1.3}$$

where T_p is the time needed by an acoustic wave to travel between the two ends of one pipe, and ω is the radian frequency. Also, using the same equation, we can describe the wave propagation through a tool joint, but instead of T_p we use T_j which is the time needed for an acoustic wave to travel between the two ends of the tool joint.

Since the pipe and the tool joint have different diameters and thicknesses, the waves that transfer from the pipe to the tool joint will lose some power by reflection, due to the mismatched impedance and the rest will be transmitted through the tool joint. The same thing happens when the acoustic wave is incident from the tool joint to the pipe, as shown in Figure 1.6. The total sum of the transmitted wave and the reflected wave equal the incident wave, with the assumption that there is no power leakage at the junction. Let t refer to the transmission coefficient and r refer to the reflection coefficient, where $t + r = 1$.

The reflection and transmission coefficients are evaluated numerically based on the parameters of the pipe and the tool joint [12]. The following matrix equation describes the acoustic wave propagation at the junction between the pipe and the tool joint

$$\begin{bmatrix} U_j \\ D_j \end{bmatrix} = \frac{-1}{t_j} \begin{bmatrix} -1 & r_p \\ -r_j & r_j r_p - t_j t_p \end{bmatrix} \begin{bmatrix} U_p \\ D_p \end{bmatrix} \tag{1.4}$$

where

$$M_{pj} = \frac{-1}{t_j} \begin{bmatrix} -1 & r_p \\ -r_j & r_j r_p - t_j t_p \end{bmatrix} \tag{1.5}$$
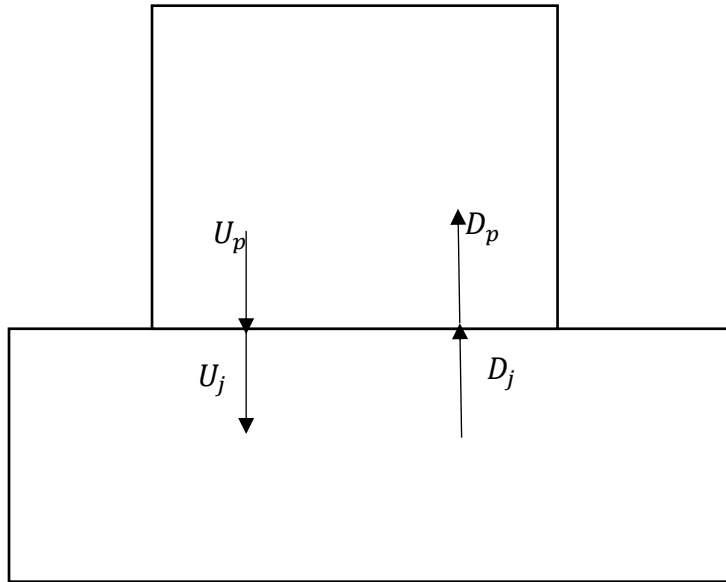
Figure 1.6 Acoustic wave propagation through the interface between pipe and tool joint.

represents the transformation matrix from the pipe to the tool joint. On the other hand, the matrix that describes the wave propagation at the junction from the tool joint to the pipe is

$$M_{jp} = \frac{-1}{t_p} \begin{bmatrix} -1 & r_j \\ -r_p & r_p r_j - t_p t_j \end{bmatrix}$$

(1.6)

Assume we have a drill string consisting of N pipes and $N-1$ tool joints, by using matrix multiplication operation and the matrix equations above, we can model the acoustic wave propagation through the drill string as follows

$$\begin{bmatrix} U_1 \\ D_1 \end{bmatrix} = M_p^1 M_{pj}^1 M_j^1 M_{jp}^1 M_p^2 ... M_{pj}^{N-1} M_j^{N-1} M_{jp}^{N-1} M_p^N \begin{bmatrix} U_N \\ D_N \end{bmatrix}$$

(1.7)

Equation (1.7) is a matrix, which contains four unknowns and two equations; and thus, we need to specify two further equations to be able to solve equation (1.7) for the unknown variables. We need to add two equations from the boundary conditions of the drill string. Assume an acoustic wave impulse transmitted through the drill string with amplitude C_o as shown in Figure 1.4, the up-going wave at the middle of the transmitter pipe, is given by

$$U_0 = C_o e^{j\omega T_p/2} + r_o e^{j\omega T_p} D_o$$

(1.8)

where r_o is the reflection coefficient from the drill string edge at the transmitter side, U_0 and D_o are the up-going and down-going waves at the middle of the transmitter pipe. The second equation is derived from the drill string end at the receiver side as follows,

$$D_N = r_{N+1} e^{j\omega T_p} U_N \tag{1.9}$$

where r_{N+1} is the reflection coefficient from the drill string edge at the receiver side, U_N and D_N are the up-going and down-going waves at the middle of the receiver pipe. After solving Eqs. (1.7-1.9), the received acoustic wave at middle of the receiver pipe of the drill string is the summation of the up-going and down-going waves

$$R = U_N + D_N \tag{1.10}$$

The attenuation factor $e^{-\alpha T}$ can be added to the propagation matrix in Eqs. (1.2,1.3) to model the acoustic wave attenuation when the wave propagates through the drill string. We use the same dimensions used in [7] for the pipes and tool-joints in the proposed drill string model, the drill string channel frequency and impulse responses of which are shown in Figure 1.7 and Figure 1.8, respectively. We have built a testbed pipe string that consists of four pipes and three tool joints, the dimensions of which are clarified in the next section. By comparing our measured channel with the drill string channel proposed in this section, we found that the proposed drill string channel model is an ideal model, whilst in a real drill string, the pipes and tool joint junctions are not perfectly stacked on each other and there may be tiny spaces that make the propagated acoustic wave behave differently from

our assumption. To model this effect in the measured channel would be very complicated. Also, because we will study the performance of a tri-axial accelerometer receiver and strain receiver in addition to the single accelerometer, modeling the channels of these receivers is even more complex and for this we resort to the measured pipe string channels.
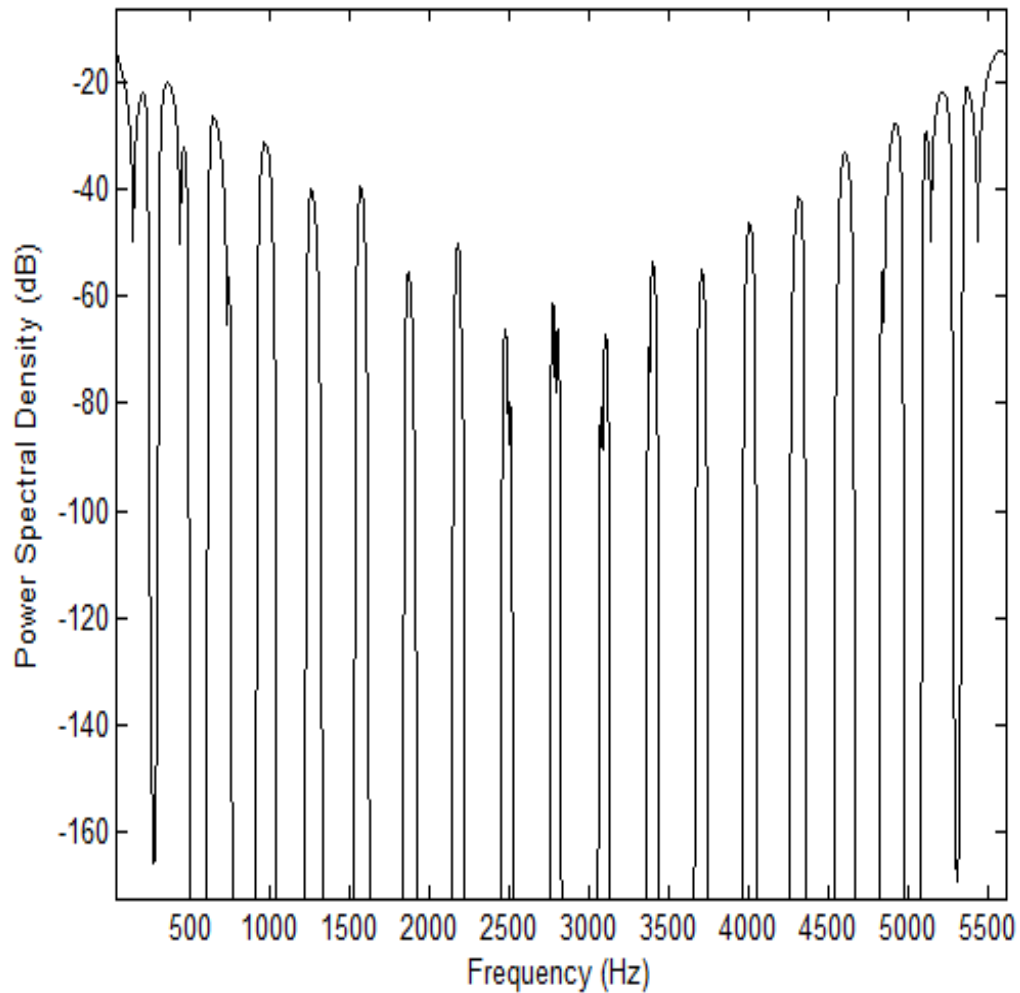
Figure 1.7 Channel frequency response of the drill-string model.
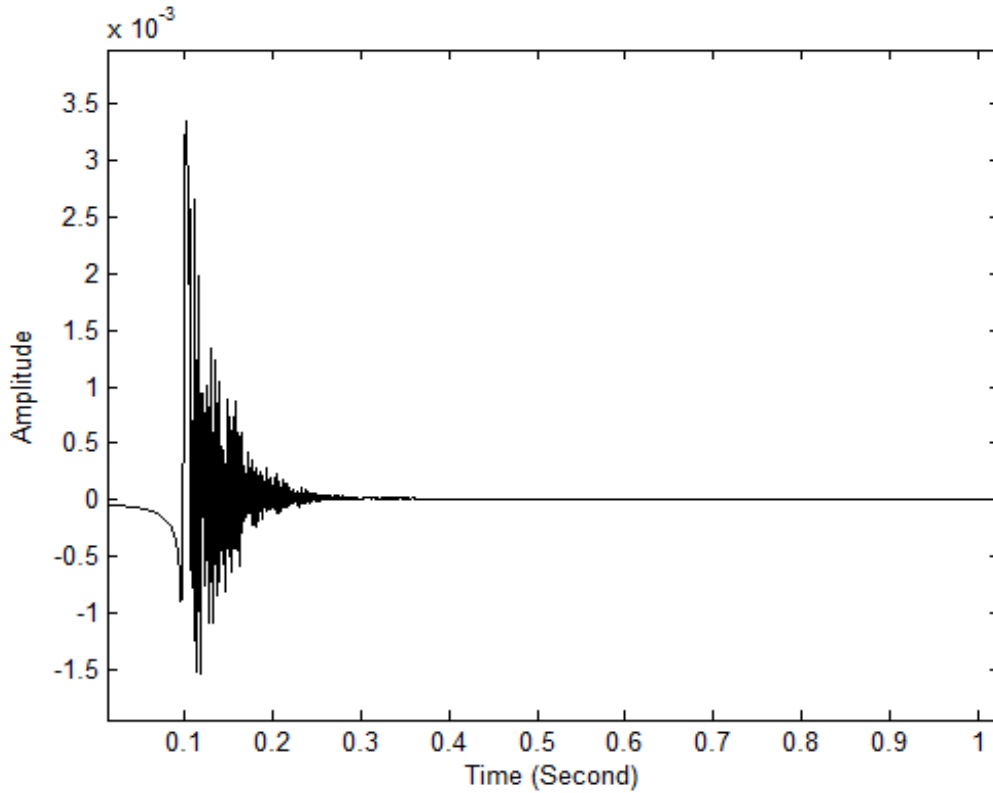
Figure 1.8 Channel impulse response of the model.

1.3 Dissertation Organization

The rest of the dissertation is organized as follows: Chapter 2 provides an overview of the testbed components, and presents the processing stages needed to obtain the baseband measured channel. In Chapter 3, we investigate the use of the tri-axial accelerometer and compare it with the uni-accelerometer. In Chapter 4, we investigate the performance of the strain receiver and compare it with the performance of a uni-acceleormeter receiver. In Chapter 5, we study the channel characteristics of the strain and tri-axial accelerometer receivers and compare their performance as a multi-channel receiver with the single-accelerometer receiver. Finally, Chapter 6 contains the discussion and conclusion.

CHAPTER 2

PIPE STRING TESTBED

2.1 Testbed Design

The main goal of this dissertation is to investigate the use of different kind of acoustic

receiver in borehole communication using an acoustic wave. For this, we have built a

testbed that consists of a transmitter unit, pipe-string, and receiver unit as shown in Figure

2.1.
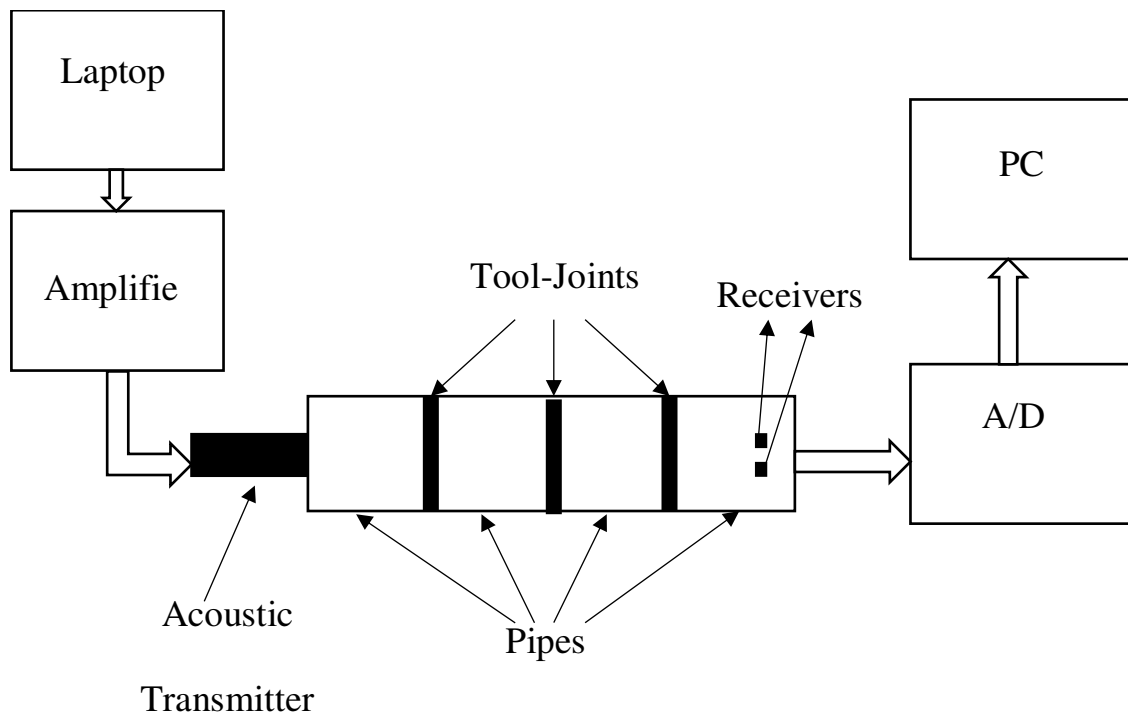
Figure 2.1 Pipe string testbed.

The chirp signal is first generated using a laptop and then fed into an amplifier. Then, the amplified signal is fed into the acoustic transmitter. The acoustic transmitter is mounted on one edge of the pipe string, and the acoustic signal that is generated by the acoustic transmitter is propagated through the pipe string that is constructed from four pipes and three tool joints. At the other end of the pipe string, several receivers are mounted on the pipe. The receivers generate analog voltage signals according to the received acoustic signal, and the analog received signal is fed into the Analog-to-Digital (A/D) device. The output samples of the A/D device are fed into another PC to be cross-correlated with the transmitted chirp signal in order to produce the measured channel impulse response. In the following, the main components of the testbed are presented in detail.

2.2 Transmitter Unit

Matlab Software was used as the platform to write the code that generates a linear modulation frequency chirp signal. A Dell laptop was used to host the Matlab software and was connected to the Analog-to-Digital Converter (ADC) through the Universal Serial Bus (USB) port. The Linear Frequency Modulated (LFM) chirp signal was selected as the probe signal to estimate the pipe string channel impulse response, where the chirp signal can be generated in the time domain as follows,

$$x_c(t) = A\cos(2\pi f(t)t + \phi), \tag{2.1}$$

where $f(t)$ is the time varying frequency given by

$$f(t) = \frac{k}{2}t + f_0 \qquad (2.2)$$

and

$$k = \frac{f_1 - f_0}{T} \qquad (2.3)$$

is the rate of frequency increase over duration T. f_1 and f_0 are the boundaries of the measured channel bandwidth. Since the generated electrical chirp signal from the laptop is weak, due to the fact that the laptop has a certain limit on the highest output power from the speaker port, we use an amplifier to amplify the generated chirp signal. Figure 2.2 and Figure 2.3 show pictures of the transmitter unit.

Figure 2.2 Amplifier.

Figure 2.3 Acoustic transmitter.

Figure 2.4 Pipe string constructed from four pipes and three tool joints.

2.3 Pipe String

The pipe string represents the medium that the acoustic waves propagate through and it is constructed from 4-inch steel pipes connected to each other using a threaded tool joint, as shown in Figure 2.4. To minimize the interface between the pipe string and the surface, the pipe string is positioned over jack stands, as shown in Figure 2.4. The acoustic transmitter is mounted on one end of the pipe string using a tool joint and a cap, and the receivers are mounted on the other end of the pipe string.

2.4 Receiver Unit

The receiver unit consists of acoustic receivers, an ADC, and a PC.

2.4.1   Acoustic Receivers

In this dissertation, there are three acoustic receivers used in the pipe string channel measurements; a single accelerometer, a tri-axial accelerometer, and a strain sensors. The output of the receiver first goes through the signal conditioner device to prepare it for next processing stage.

2.4.1.1 Single Accelerometer.   The single accelerometer used in the pipe string channel measurements is an 352C33 model provided by PCB Piezotronics. The single accelerometer voltage sensitivity is 100 mV / g and it supports the frequency range 0.5 Hz -10 kHz. In addition, a wax was used to stick the single accelerometer onto the pipe string at the required location. Figure 2.5a shows the single accelerometer.

2.4.1.2 Tri-axial Accelerometer.   The   tri-axial   accelerometer   measures   the accelerations in three dimensions X, Y, Z, hence, we have three different communication channels. The tri-axial accelerometer is a 356B21 model provided by PCB Piezotronics. The tri-axial accelerometer voltage sensitivity is 10 mV/g and it supports the frequency range $0.5\,Hz$ -$10\,kHz$. The tri-axial accelerometer is also mounted on the pipe string using wax at the required location. Figure 2.5b shows a picture of the tri-axial accelerometer.

2.4.1.3 Strain .   The strain sensor measures the change of length with respect to the original length. The strain sensor used in the pipe string channel measurements is a 740B02 model provided by PCB Piezotronics. The strain sensor voltage sensitivity is $50mV/\mu\varepsilon$ and it supports the frequency range $0.5Hz - 100kHz$. Superglue is used to stich the strain sensor onto the pipe string at the required location. A picture of the strain sensor is shown in Figure 2.5c.

2.4.2   Analog-to-Digital Convertor

The analog to digital device samples and digitizes the analog signal coming from the signal conditioner and passes those samples to the PC. The ADC used is an MC USB-1608FS-Plus card provided by Measurement Computing. This card has a maximum sampling rate of $100,000 samples/\sec$ and it uses 16 bits to digitize the samples. The card is connected to the PC using a USB cable. In the pipe string channel measurements, the received signal is sampled at $40ksamples/\sec$. The ADC device is shown in Figure 2.6.

Figure 2.5 a) Single accelerometer. b) Tri-axial accelerometer. c) Strain sensor.

2.4.3 Computer Hardware and Software

MATLAB software was used to capture, save, display, and analyze the channel measurements. A DELL desktop computer was used to host the MATLAB software and connect the ADC through the USB port. This computer run on Windows 7, has 4 GB of RAM memory, and its processor is an Intel Core 2 Duo CPU that runs at 2.93 GHz.

2.4.4 Signal Analysis

The received signal is cross-correlated with the transmitted chirp signal to produce the channel impulse response. After the pipe string channel measurements are collected from the testbed, there are two further stages before the measurements can be used in borehole communication performance analysis. First, we need to remove the background noise and second, we need to convert it to a complex baseband channel.

Figure 2.6 Analog-to-Digital converter (ADC).

2.4.5 Noise Rejection

In addition to the transmitted chirp signal, the acoustic receiver also receives additive noise due to thermal and background noise. To reduce the noise effect on the pipe string channel impulse response, we need to set a threshold level to reject the background noise. The channel impulse taps that have an amplitude of less than this threshold will be set to zero. Figure 2.7 shows the pipe string power delay profile with the noise threshold level.
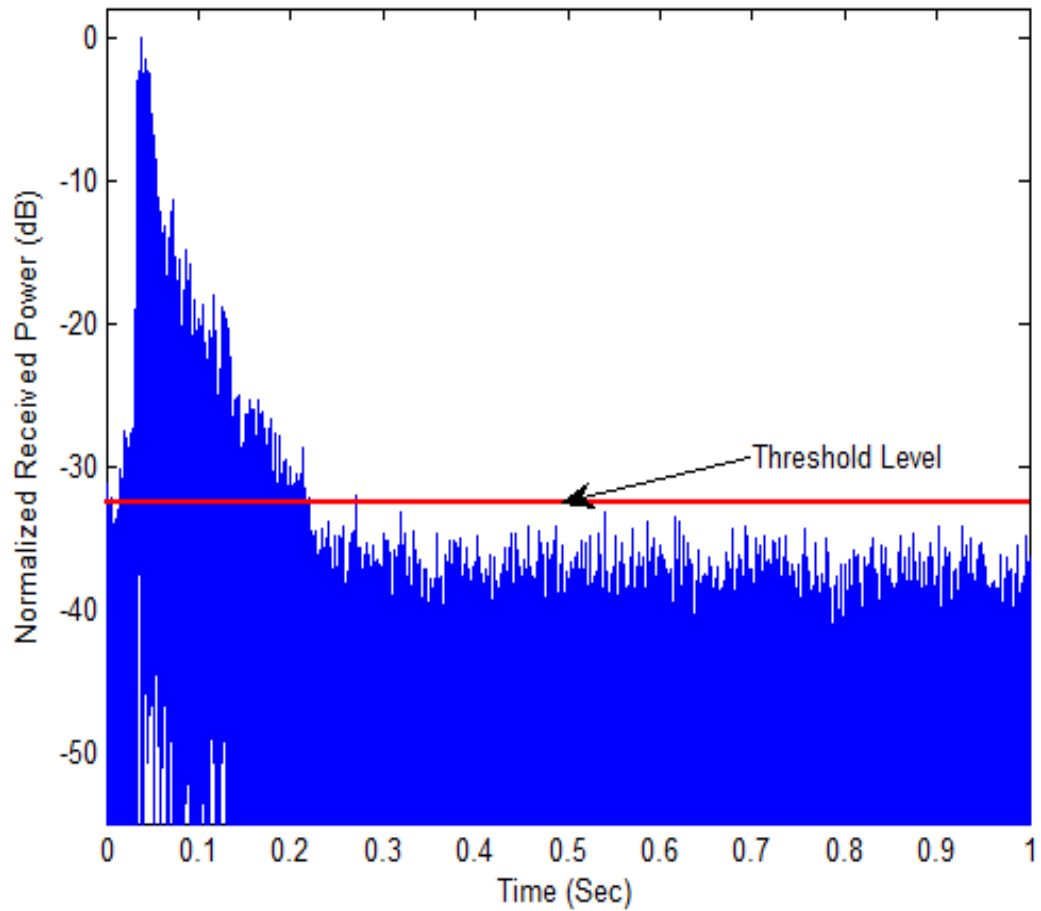
Figure 2.7 Set a threshold to reject the additive noise.

2.4.6 Complex Baseband Channel

For the last step before use of the measured channel in the performance analysis, we convert the bandpass channel into a complex baseband channel. The resulting measured pipe string channel $h(t)$ from the testbed is the bandpass channel in the frequency domain for which all frequency components are located around a central frequency $|f_c|$, as shown in Figure 2.8, which shows a real signal in the time domain.
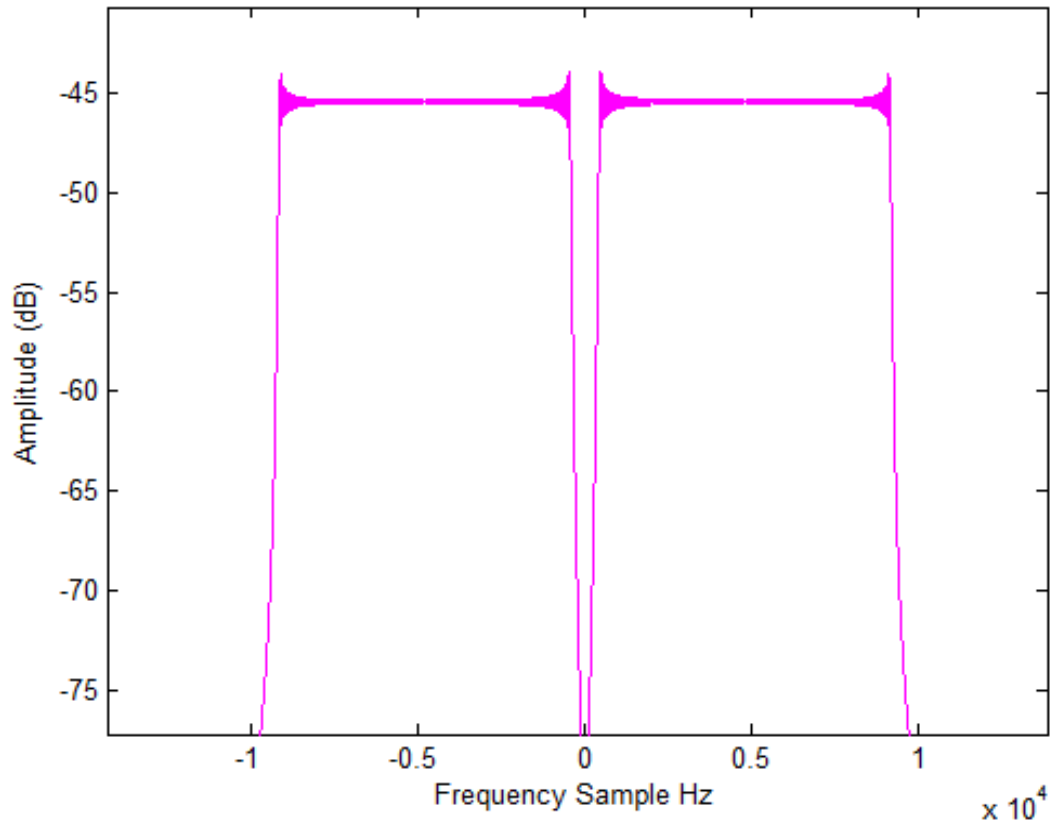
Figure 2.8 Bandpass channel in frequency domain.

To convert the bandpass channel to a baseband channel, first, we determine the Hilbert transform of the bandpass channel $h(t)$, as follows

$$h_H(t) = h(t) \otimes \frac{1}{\pi t} \tag{2.4}$$

where $\otimes$ the convolution operation. Then, the baseband channel is

$$h_{BP}(t) = [h(t) + h_H(t)]e^{-j2\pi f_c} \tag{2.5}$$

The resulting baseband channel is shown in Figure 2.9.
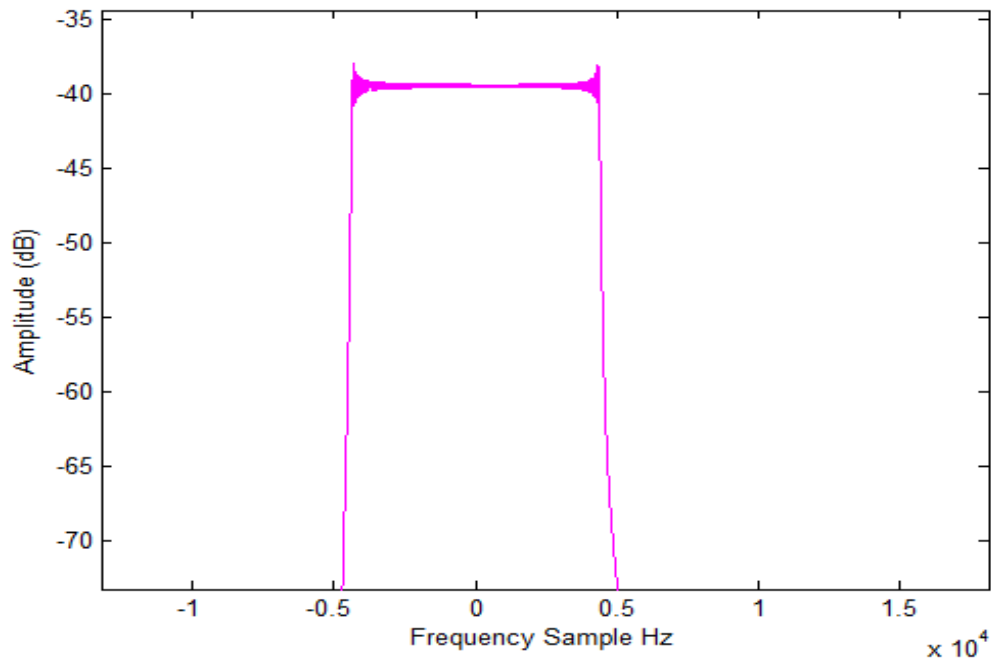
Figure 2.9 Resulting baseband channel in frequency domain.

CHAPTER 3

A COMPARATIVE STUDY OF MULTICHANNEL AND SINGLE CHANNEL ACCELEROMETER SENSORS FOR COMMUNICATION IN OIL WELLS

Signal reception using multichannel devices and multiple receivers is known to be a useful means to improve communication system performance in multipath environments [13]. However, in various propagation environments, such as acoustic channels [14] and radio frequency channels [15], there might be correlations between the multiple channels of a receiver which may affect the system performance. These possible correlations need to be well understood, before the deployment of a multichannel receiver.

Single channel accelerometers have been widely used for signal reception in drill string communication systems. One can envision using more than one single channel accelerometer for multiple signal reception. Another alternative for multiple signal reception to use a multichannel accelerometer which measures and provides several different acceleration signals, as explained in the following section. The goal of this chapter is to study these two multi-reception schemes in the context of drill string communication systems in order to understand and compare possible levels of correlations between the channels.

The technical challenge is due to the fact that, because of many back and forth signal reflections between tool joints throughout the drill string, analytical modeling and simulation of signal propagation in drill strings are complex tasks and involve partial differential equations with proper boundary conditions [12]. These become more complicated when there are multiple sensors and multichannel sensors, with possible correlations, which are the focus of this chapter. Therefore, as a plausible approach, we

resort to experiments to obtain a picture of the possible correlations among various acceleration signals in drill strings.

In this chapter, we study the performance of multichannel and single channel accelerometers used as uphole communication receivers. Using experimental results from a drill string communication testbed, we show that one tri-axial accelerometer can provide nearly uncorrelated signals, compared to two single channel accelerometers. Having uncorrelated signals at the uphole receiver provides diversity, which in turn can result in an increase in the communication system's performance.

The rest of this chapter is organized as follows. In Section II various types of acceleration signals are introduced and equations for the received signals resulting from convolution of the transmitted signal with drill string channel impulse responses are provided. The experimental testbed is presented in Section III, whereas the drill string channel impulse response measurements are provided in Section IV. Section V discusses correlations among various types of measured channels and how they affect the system performance. Concluding remarks are given in Section VI.
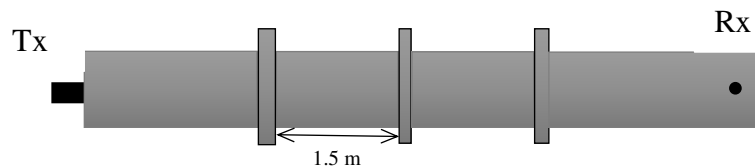
Figure 3.1 The drill string testbed, not drawn to scale. The transmitter (black rectangle) is on the   left, whereas accelerometers are mounted on the right, at the end of the last pipe.

3.1 Acceleration Signals Sensed by Accelerometers

Let an acoustic transducer be placed on one end of a drill string, which generates the signal $\gamma(t)$ by converting information from electric form to acoustic waves. These acoustic waves travel through the drill string, and are sensed by an accelerometer at the other end of the drill string. The accelerometer is a sensor that converts acoustic waves to electric signals. The multichannel sensor that we consider in this paper is a tri-axial accelerometer which measures accelerations of local vibrations at a single point in three orthogonal directions x, y, and z. Let $u_x(t)$, $u_y(t)$ and $u_z(t)$ be the time-varying local displacements due to vibrations at a single point at the end of the drill string, where the accelerometer is mounted. With acceleration as the second derivative of displacement with respect to time [12], the three acceleration signals can be written as

$$a_i(t) = \partial^2 u_i(t) / \partial t^2, \quad i = x, y, z.$$ (3.1)

The vector nature of the tri-axial sensor that measures the orthogonal components of acceleration resembles the vector sensor receiver in [18] which measures orthogonal particle velocity components.

Let the three drill-string channel impulse responses, which correspond to the tri-axial accelerometer receiver, be represented by $h_x(t), h_y(t)$ and $h_z(t)$. Upon transmitting the signal, $\gamma(t)$, the three received signals can be written as

$$r_i(t) = h_i(t) \oplus \gamma(t) + n_i(t) \,, \quad i = x, y, z \,.$$ (3.2)

where $\oplus$ stands for convolution and $n_i(t)$ represents noise in the i-th channel. In the next section we present our drill string communication testbed, and then in Section 3.3 we show how the three channel impulse responses in equation (3.2) can be obtained from the acceleration measurements of the sensor given in equation (3.1).

Figure 3.2 The transmit transducer mounted along the drill string testbed axis.

3.2 The Drill String Testbed

The drill string testbed consists of four steel pipes connected via tool joints, as schematically shown in Figure 3.1. The length and diameter of each pipe are 60 and 4 inches, respectively (about 1.5 m and 10 cm, respectively). The length of each tool joint is 3.5 inches (about 9 cm). The transmitter is a magnetostrictive transducer that can generate vibrations of up to 20 kHz. The actual testbed and the transmitter are shown in Figure 3.2. In Figure 3.3, the mounted tri-axial accelerometer is shown on the receiver side.
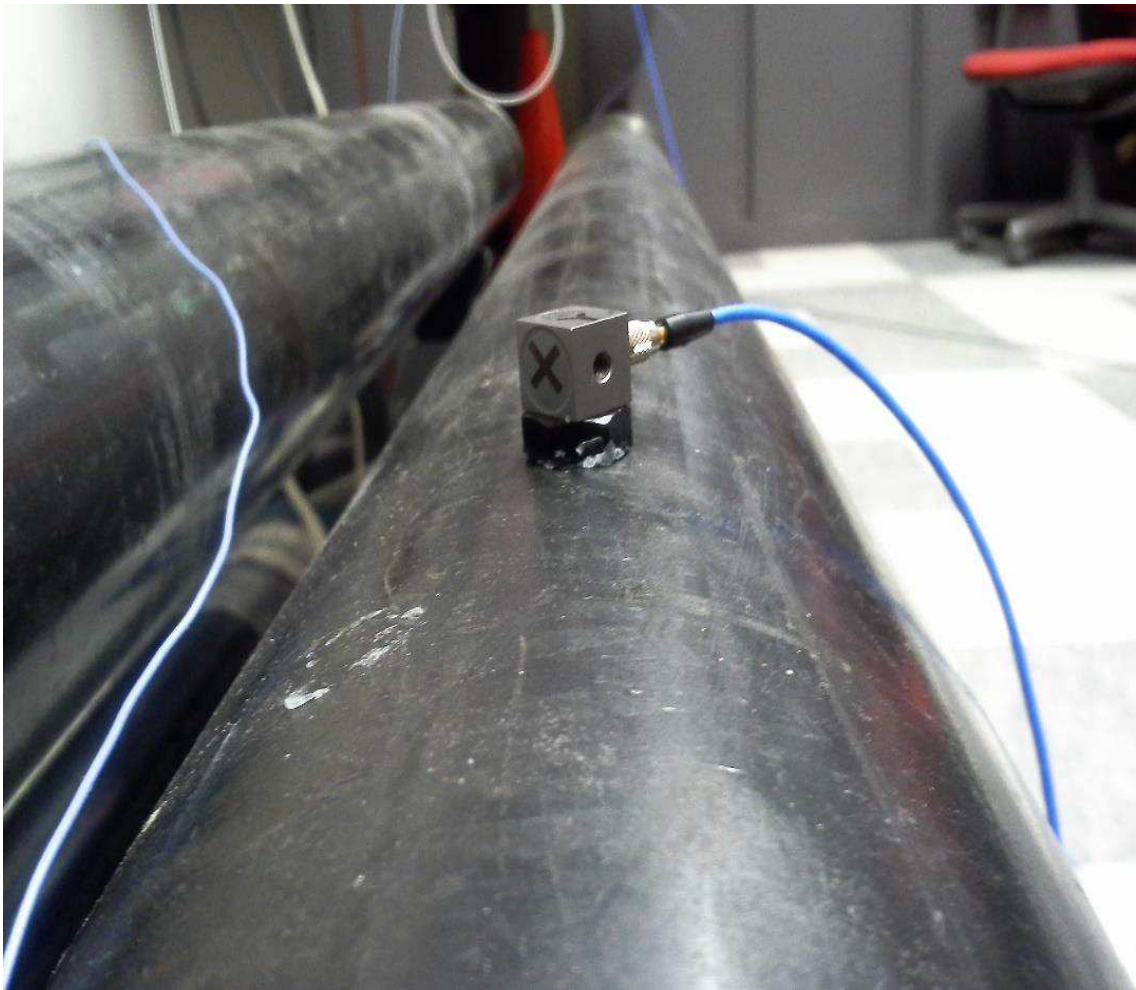
Figure 3.3 The tri-axial accelerometer mounted on the receiver side.
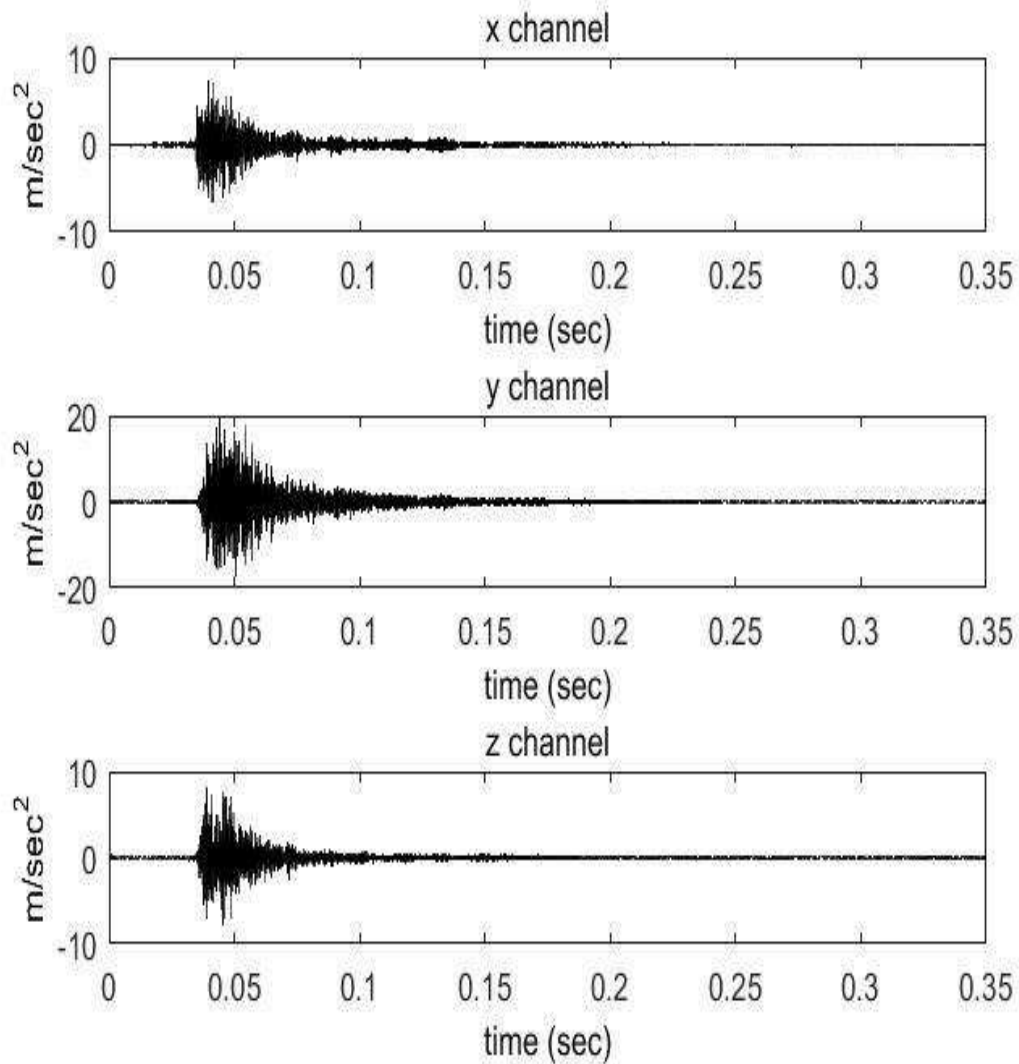
Figure 3.4 Drill string channel impulse responses measured by a tri-axial accelerometer.

3.3 Drill String Channel Impulse Responses

To measure the drill string channel impulse responses sensed by the accelerometers, the

drill string is excited by a linear frequency-modulated chirp signal of duration 1 sec. over

the frequency range of 0.4 to 9.2 kHz. The chirp signal is generated by a computer,

amplified by a power amplifier, and then applied to the transmit transducer. At the receiver

side, signals measured by the accelerometers are collected and sampled at a rate of 40 ksamples/sec using a multichannel analog-to-digital converter and then fed into another computer. Cross-correlation of the received signals with the original chirp signal provides measurements of the channel impulse responses in the drill string.
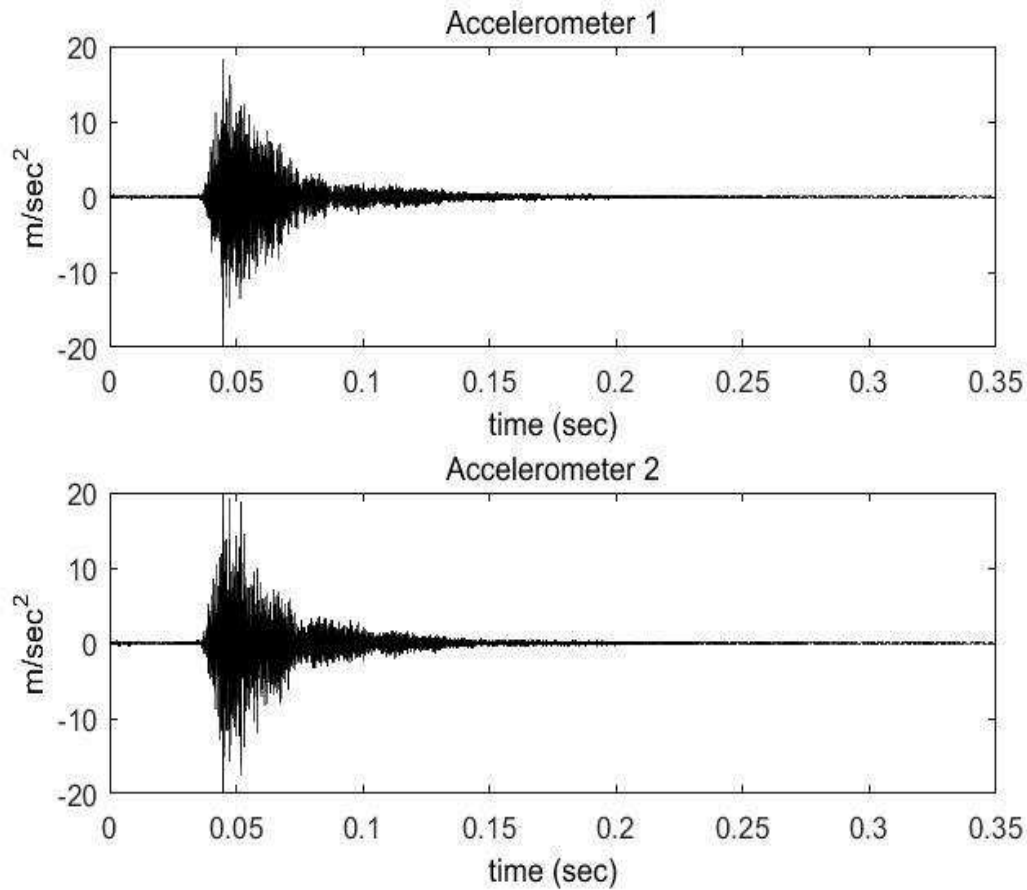
Figure 3.5 Drill string channel impulse responses measured by two single channel accelerometers.

For the tri-axial accelerometer, the sensitivity per channel is $\beta = 10$ milliV/g, where g $= 9.8$ m/sec^2 is the gravitational acceleration, whereas for the single channel accelerometer we have $\beta = 100$ milliV/g. To account for different sensor sensitivities, the readouts of the accelerometers, which are in milliV, are multiplied by the factor g / β,

which converts the units to m/sec^2. The three channel impulse responses $h_x(t)$, $h_y(t)$ and $h_z(t)$ measured by the tri-axial accelerometer are shown in Figure 3.4. The channel impulse responses $h_1(t)$ and $h_2(t)$ measured by two adjacent single channel accelerometers are shown in Figure 3.5.

3.4 Channel Correlations and System Performance

In this section, we calculate channel impulse response correlations for two different receivers. Receiver A is a tri-axial accelerometer, whereas receiver B is composed of two single channel accelerometers.

After converting real passband channel impulse responses to complex baseband equivalents, correlation magnitudes between the channels of the above two receivers are calculated and listed in Table 3.1. It appears that channels in the tri-axial accelerometer are nearly uncorrelated, whereas the two single channel accelerometers are highly correlated. This indicates that the multichannel accelerometer can serve as a better communication receiver compared to the two single channel accelerometers.

To better understand how a high correlation level among channel impulse responses with complex multipath structures can affect communication system performance, one can look at the condition number and eigen spectrum of the matrix $\mathbf{H}^\dagger\mathbf{H}$, where $\mathbf{H}$ is the entire system channel matrix and † stands for transpose conjugate. These metrics can be used to compare the performance of multichannel equalization in communication receivers utilizing different channels [16] [17]. In another chapter we use the bit error rate to compare the performance of the receivers utilizing different types of accelerometers.

Table 3.1 Measured Channel Correlation Magnitudes for Two Receivers: Receiver A is a Tri-axial Accelerometer, whereas Receiver B Consists of Two Single Channel Accelerometers.

Receiver A		Receiver B	
Correlation of $h_x(t)$ and $h_y(t)$	0.25		
Correlation of $h_x(t)$ and $h_z(t)$	0.25	Correlation of $h_1(t)$ and $h_2(t)$	0.73
Correlation of $h_y(t)$ and $h_z(t)$	0.1		

Let $\mathbf{H}_i$, $i = x, y, z, 1, 2$, be the i-th banded channel matrix whose dimension is $(K + M - 1) \times K$ [16]

$$\mathbf{H}_i = \begin{bmatrix} h_i(0) & & & \\ \vdots & \ddots & h_i(0) & \\ & & & \vdots \\ h_i(M-1) & \ddots & & \\ & & h_i(M-1) \end{bmatrix} \tag{3.3}$$

where M is the number of channel taps and K is the number of transmitted symbols.

Similarly to [16], the entire system channel matrices for the tri-axial accelerometer system, receiver A, and the system with two single channel accelerometers, receiver B, are given by

$$\mathbf{H_A} = \begin{bmatrix} \mathbf{H}_x \\ \mathbf{H}_y \\ \mathbf{H}_z \end{bmatrix}, \qquad \mathbf{H_B} = \begin{bmatrix} \mathbf{H}_1 \\ \mathbf{H}_2 \end{bmatrix} \qquad\qquad (3.4)$$

The condition number of a matrix is the ratio of its largest singular value to the smallest singular value. A large condition number indicates that the channel matrix is nearly singular, which translates into more difficult and less effective equalization [16]. For $K = 100$ transmitted symbols, condition numbers for $\mathbf{H_A^\dagger H_A}$ and $\mathbf{H_B^\dagger H_B}$ according to (3.4), calculated using Matlab, are 9.8×10^3 and 18.7×10^3, respectively. The smaller condition number for the tri-axial accelerometer system, receiver A, can be attributed to its nearly uncorrelated channels, as listed in Table 3.1. On the other hand, the high channel correlation in Table I for the system with two single channel accelerometers, receiver B, can be related to the larger condition number. Typically, a smaller condition number, such as system A's, results in more effective equalization and a lower bit error rate [16].
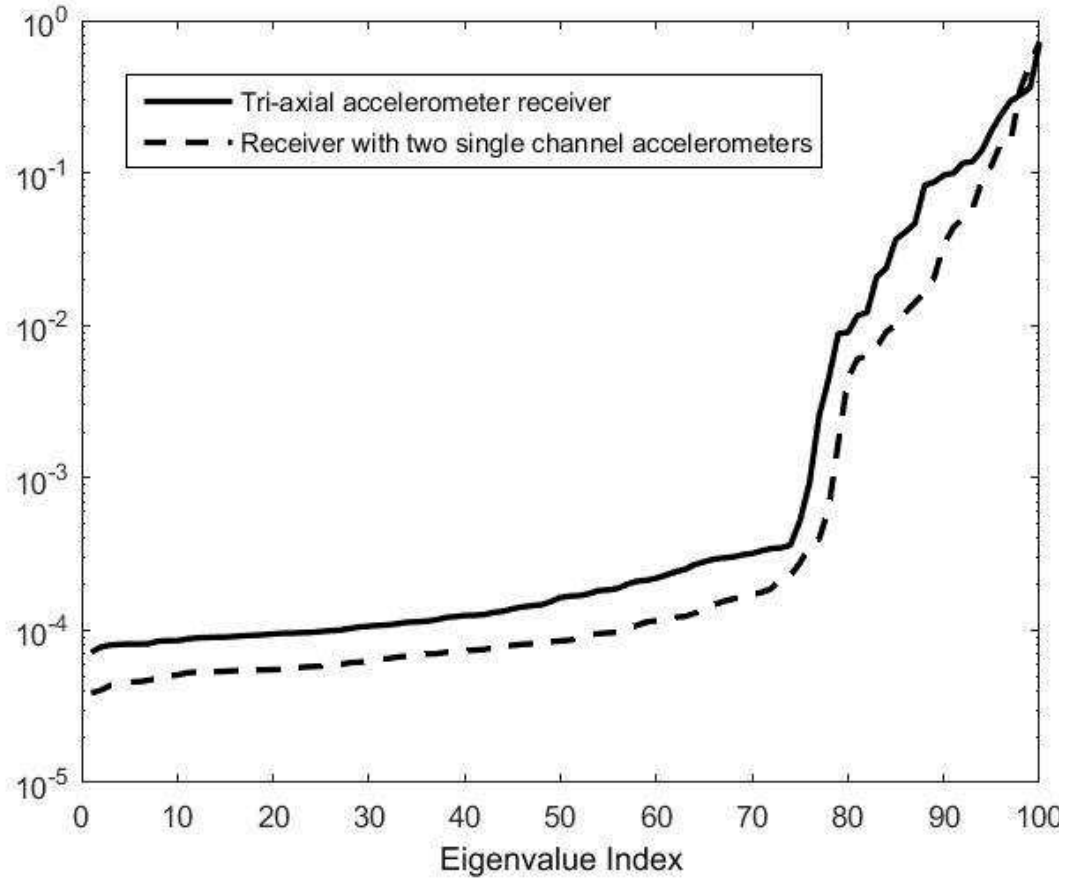
Figure 3.6 Normalized sorted eigenvalues of $\mathbf{H}_A^\dagger \mathbf{H}_A$ and $\mathbf{H}_B^\dagger \mathbf{H}_B$ for two receivers: receiver A is a tri-axial accelerometer, whereas receiver B consists of two single channel accelerometers.

The better performance of the tri-axial accelerometer, system A, can also be viewed from another angle. In Figure 3.6 eigenvalues of $\mathbf{H}_A^\dagger \mathbf{H}_A$ and $\mathbf{H}_B^\dagger \mathbf{H}_B$ are plotted for the two systems A and B, respectively. Eigenvalues for each system are normalized such that the largest eigenvalue is 1. We observe that the eigenvalues of the tri-axial accelerometer receiver are greater than those of the receiver which consists of two single channel accelerometers. As discussed in [16], the performance of a system with larger eigenvalues is better due to its more effective equalization. This reflects the value of the tri-axial

receiver which benefits from co-located, yet nearly uncorrelated, channels as listed in Table

3.1.

CHAPTER 4

EXPERIMENTAL RESULTS ON ACOUSTIC COMMUNICATION THROUGH A DRILL STRINGS USING A STRAIN SENSOR RECEIVER

The receiver sensor usually used in the experimental study of acoustic communication through a drill string is the acceleration sensor that measures the acceleration of the received acoustic wave [7], [22], and [23]. In this chapter, we investigate the performance of the strain receiver and compare its performance with the acceleration receiver experimentally.

The chapter is organized as follows. First, we present the physical relation between the strain and the acceleration quantities, then we present the drill string testbed used for channel measurements. The performance analysis of the strain and acceleration receivers is presented in Section 4.2, and the channel dispersion parameters is given in Section 4.3.

4.1 Drill String Channel Characteristics

4.1.1   Definitions of Acceleration and Strain

There are different acoustic sensors that can be used to receive the transmitted acoustic waves that propagate through a drill string. The accelerometer and strain sensor are two sensors that measure different quantities of the acoustic wave. Assume an acoustic displacement wave $u(t)$ propagating through a drill string, the accelerometer receiver measures the second derivative of the displacement wave with respect to time, as follows

$$a(t) = \partial^2 u(t) / \partial t^2 \qquad (4.1)$$
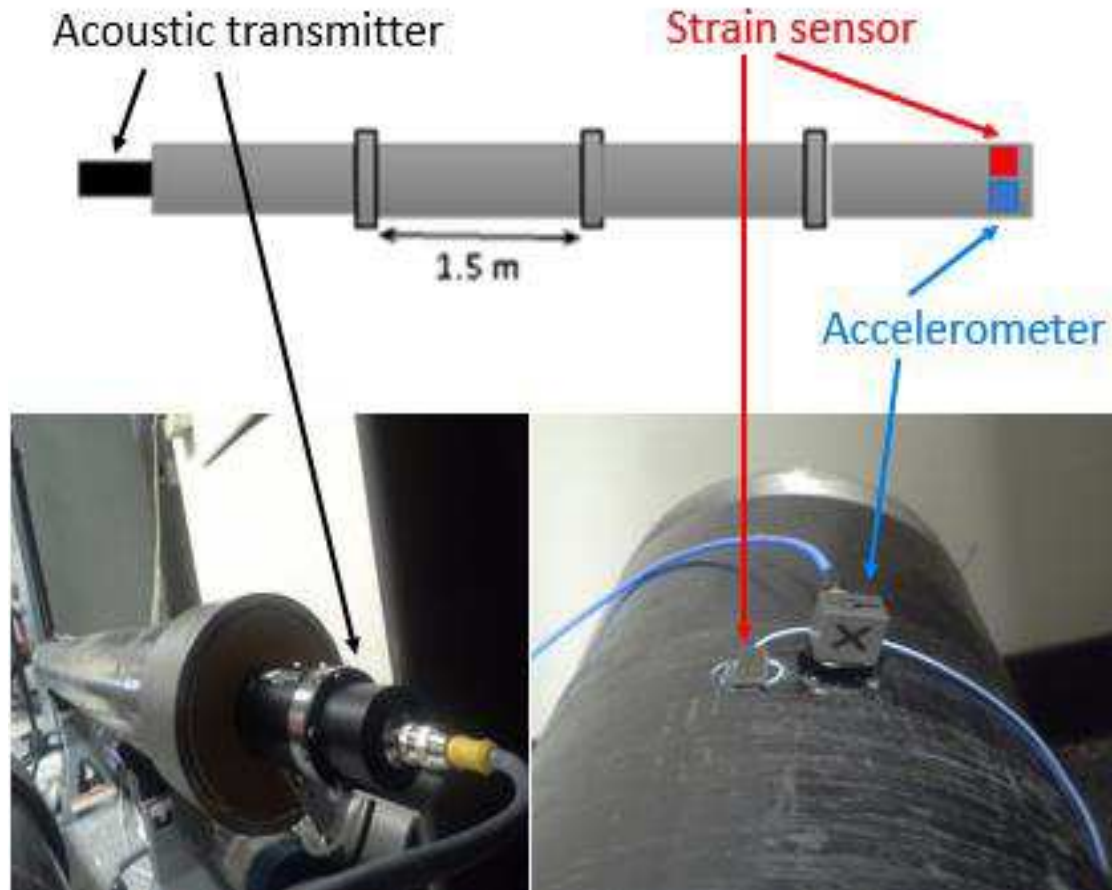
Figure 4.1 The acoustic transmitter and the accelerometer and strain sensor on the drill string.

For diversity purposes, we use a strain receiver that measures different acoustic quantities of the vibrated particles. The strain receiver measures the first derivative of the displacement wave with respect to the propagation axis,

$$s(t) = \partial u(t) / \partial x \qquad (4.2)$$

where x is the propagation axis.

4.1.2 Drill String Testbed and Measurements

The drill string consists of four pipes that are connected to each other by four tool joints, all of which are made from steel, and the pipe and tool-joint dimensions are clarified in Table 4.1. At one end of the drill string we placed an acoustic actuator such that the acoustic wave propagates longitudinally through the drill string and at the other end of the drill string we mounted the accelerometer and strain receivers beside each other, as shown in Figure 4.1.

Table 4.1 The Drill String Components Characteristics.

	Length	Diameter	Thickness
Pipe	1.5 m	10 cm	0.5 cm
Tool joint	9 cm	11 cm	0.5 cm

To measure the channel impulse responses of the accelerometer and strain receivers, a linear frequency-modulated chirp signal with 1 sec duration over a frequency range of 0.4 to 9.2 kHz is transmitted through the dill string. The chirp signal is generated by a computer, amplified by a power amplifier, and then applied to the transmit transducer. At the receiver side, signals measured by the accelerometer and strain sensor are collected

and sampled at a rate 40 ksamples/sec using a multichannel analog-to-digital converter and then fed into another computer. Cross-correlation of the received signals with the original chirp signal provides measurements of the channel impulse responses in the drill string.

The acceleration and strain sensors measure different physical quantities with different units, and in such scenarios, when different types of signals are used in a multichannel receiver they should be converted to the same unit [18].
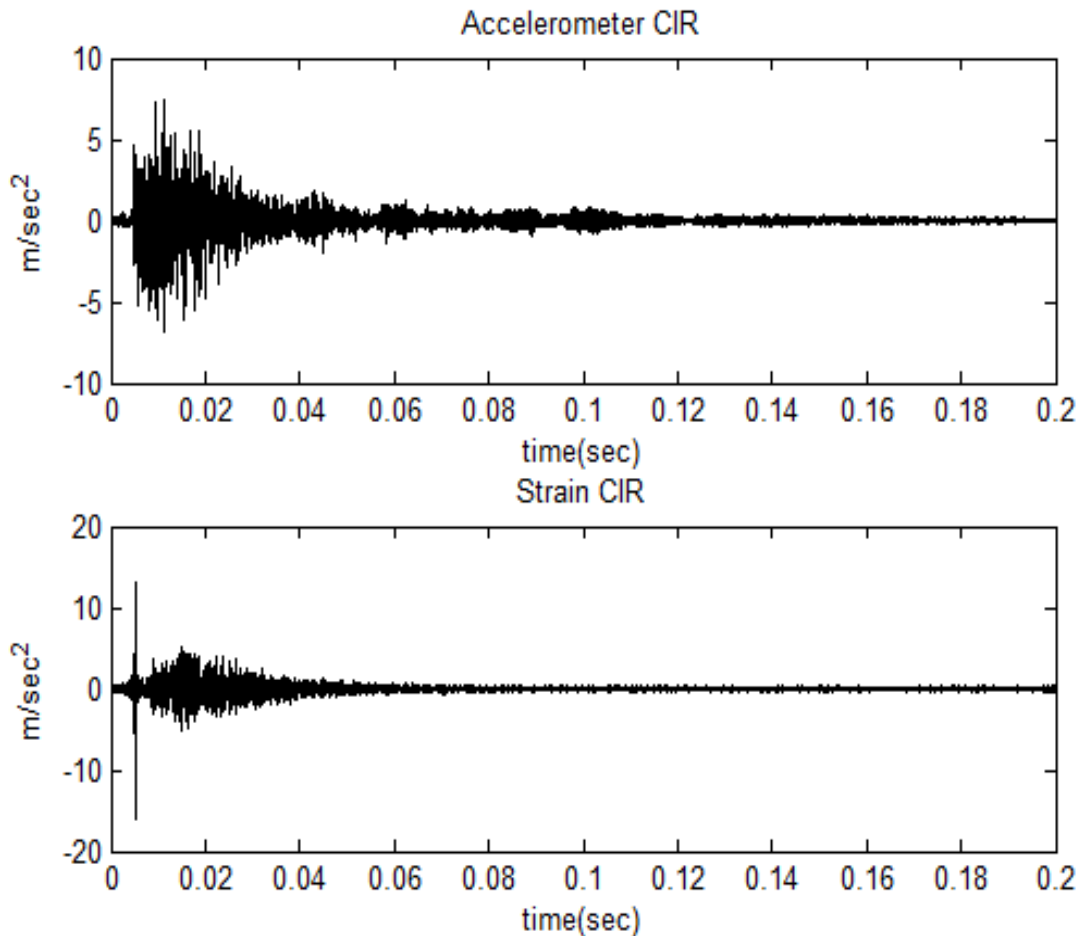
Figure 4.2 The channel impulse responses for the accelerometer and strain receivers.

The unit of acceleration is m/sec^2, whereas strain, in (4.2), is dimensionless. However, since typically its value is much smaller than one, for convenience it is usually presented in the dimensionless $\mu\varepsilon$ unit, where $1\mu = 10^{-6}$ and ε refers to strain. Additionally, sensor sensitivities are not the same and have different units as well: the unit of accelerometer sensitivity β_a is milliV/g, where g = 9.8 m/sec^2 is the gravitational acceleration, whereas the unit of strain sensor sensitivity β_s is milliV/$\mu\varepsilon$. To unify these different units, we find it useful to convert strain to acceleration. Similarly to [22], consider a plane wave for the displacement signal along the pipe axis, i.e., $u_x(t) = \exp(j(\omega t - kx))$, where $j^2 = -1$, ω is the angular frequency and k is the wavenumber. With $k = \omega / V$ in nondispersive media, where V is the wave speed, substitution of $u_x(t)$ into (4.2) results in $s(t) = (-j/V)\omega u_x(t)$. Using (4.1) we similarly obtain $a_x(t) = -\omega^2 u_x(t)$. Putting these together yields $a_x(t) = -Vj\omega s(t)$. Therefore, a differentiator filter can be used to convert strain to acceleration [24].

Upon taking the derivative of the readout of the strain sensor, which is in milliV, multiplying it by $-V$, and then by the factor $10^{-6} / \beta_s$ we convert the strain unit to m/sec^2 as well. For sensor sensitivities we have $\beta_a =$ 100 milliV/g per channel and $\beta_s = 50$ milliV/$\mu\varepsilon$. Figure 4.2 shows the accelerometer and strain impulse responses of the drill string channels.

4.2 Strain and Accelerometer Measured Drill Channels Performance Comparison

To compare the performance of the strain receiver with the accelerometer receiver, we looked at the eigen spectrum of the matrix $\mathbf{H}^{\dagger}\mathbf{H}$, where $\mathbf{H}$ is the entire system channel matrix and † stands for transpose conjugate.
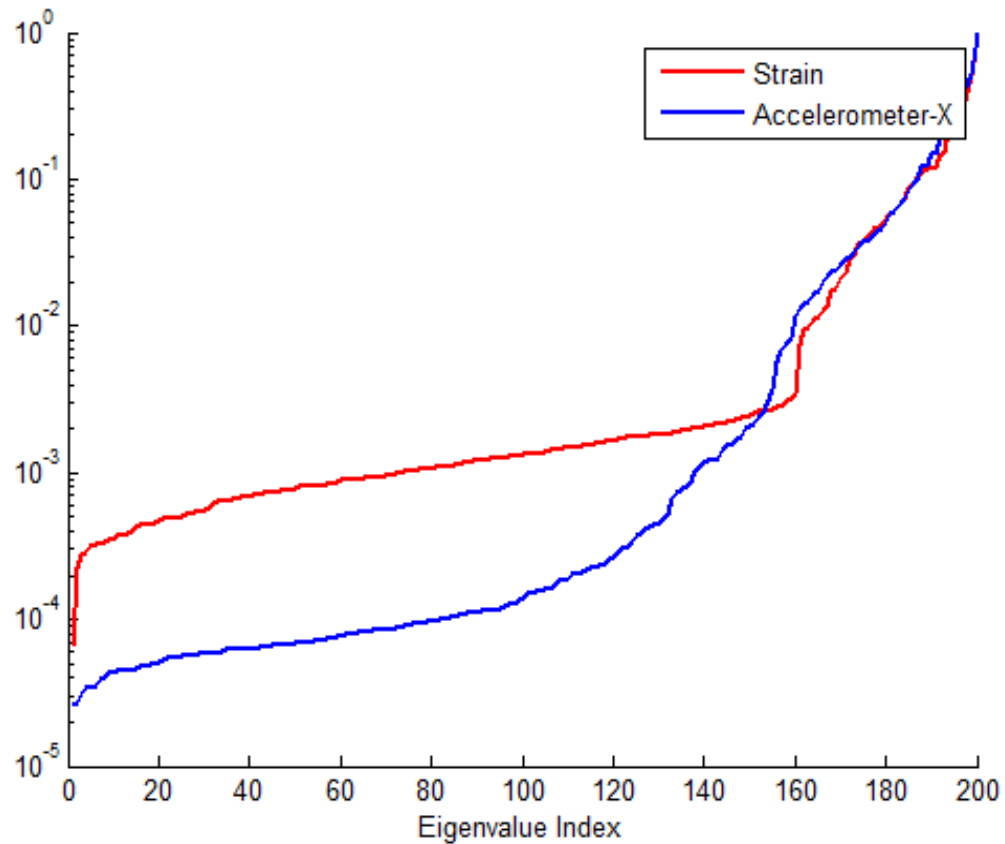
Figure 4.3 Normalized sorted eigenvalues of $\mathbf{H}_s^{\dagger}\mathbf{H}_s$ and $\mathbf{H}_a^{\dagger}\mathbf{H}_a$ for two receivers: receiver s is the strain, whereas receiver a is the accelerometer.
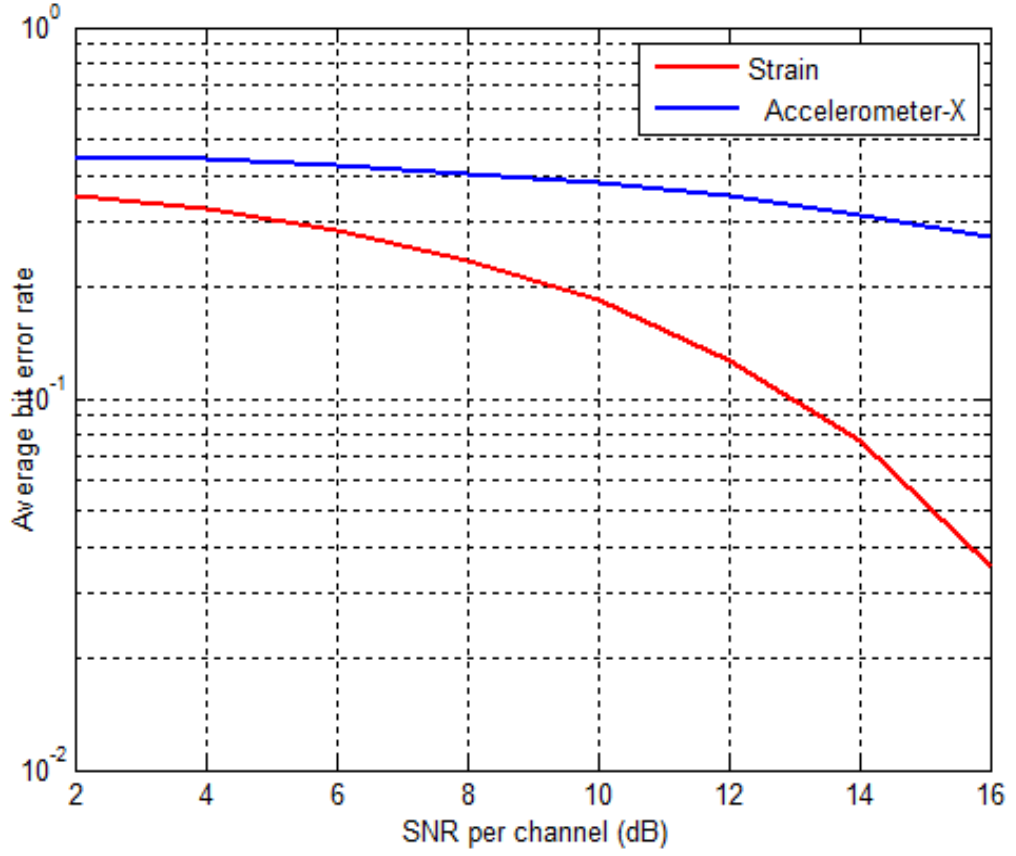
Figure 4.4 Average bit error rate of two different receivers on the drill string channel.

The banded channel matrix $\mathbf{H}$ with dimension $(K+M-1)\times K$,

$$\mathbf{H}_i = \begin{bmatrix} \tilde{h}_i(0) & & & \\ \vdots & \ddots & \tilde{h}_i(0) & \\ \tilde{h}_i(M-1) & \ddots & \vdots & \\ & & \tilde{h}_i(M-1) \end{bmatrix} \quad i=a,s \qquad (4.3)$$

where M is the number of the channel taps and K is the number of transmitted symbols, and a and s stand for acceleration channel and strain channel, respectively. The plot of the

eigenvalue of the strain matrix channel $\mathbf{H}_s{}^\dagger\mathbf{H}_s$ and acceleration matrix channel $\mathbf{H}_a{}^\dagger\mathbf{H}_a$ are shown in Figure 4.3. The eigenvalues are normalized such that the largest eigenvalue is 1. The matrix channel with the larger eigenvalue will have better performance due to its more effective equalization. This reflects the superiority of the strain receiver over the acceleration receiver.

We also investigate the performance of strain and the acceleration receivers in terms of Bit Error Rate (BER). Figure 4.4 shows the performance of the strain and accelerometer receivers on the drill string channel. This superiority of performance of the strain channel over the acceleration channel can be explained in terms of the channel structure. Figure 4.2 shows the channel impulse responses of the acceleration and strain receivers respectively. We can notice that most of the strain channel power is focused on fewer taps compared with the acceleration channel power that is spread over a larger number of taps.

4.3 Channel Time Dispersion Parameters

The root-mean-square (RMS) delay spread σ_τ is an important parameter for characterization of wireless channels and quantifies the spread of the arrival times of incoming waves from different paths [25]. It is defined by

$$\sigma_\tau = \sqrt{\overline{\tau^2} - \overline{\tau}^2} \tag{4.4}$$
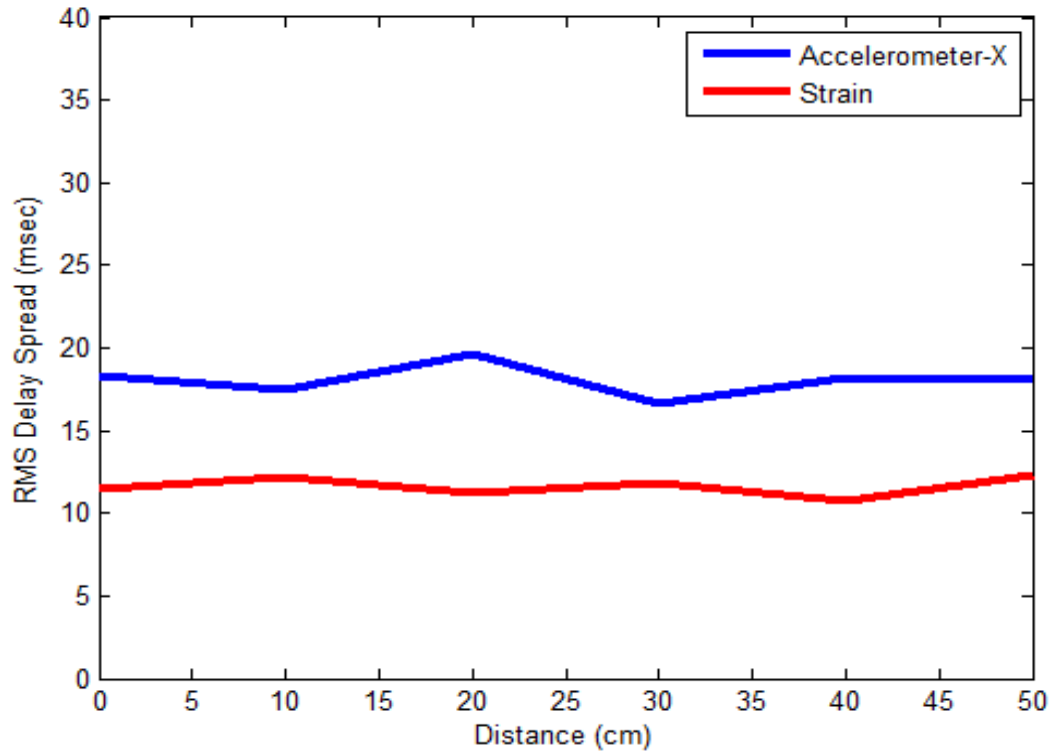
Figure 4.5 RMS delay spread of the strain and acceleration channels at different positions.

where $\bar{\tau}$ is the mean access delay of the channel impulse response given as follows

$$\bar{\tau} = \frac{\sum\limits_{k} y_k^2 t_k}{\sum\limits_{k} y_k^2} \tag{4.5}$$

and

$$\bar{\tau^2} = \frac{\sum\limits_{k} y_k^2 t^2{}_k}{\sum\limits_{k} y_k^2} \tag{4.6}$$

Figure 4.5 shows the RMS delay spread of the strain and acceleration channels at different positions on the last pipe of the drill string. We can notice from Figure 4.5 that the strain channel have less RMS delay spread than the acceleration channel, which allows for a higher bit rate for the strain channel without inter-symbol interference.

CHAPTER 5

ON MULTIPLE WIRELESS CHANNELS IN OIL WELL DRILL STRINGS

A drill string is constructed from a series of pipes connected via tool joints. Due to the mismatch between the pipes and tool joints, there are many forward and backward reflections of the transmitted signal, which result in a complex multipath channel in the drill strings. Multichannel reception using several receivers is known to be an effective approach for improving communication system performance in multipath environments [13]. However, it is observed that in various environments, such as wireless acoustic channels [14] and wireless radio frequency channels [15], there might be correlations between multiple receivers that can affect the system performance. Our goal is to study multiple wireless channels in drill strings in order to understand possible levels of correlation between such channels.

Due to many back and forth signal reflections from tool joints [12], the analysis of wave propagation in drill strings is complex and involves solving several partial differential equations, and superpositions of several wave modes expressed as functions of eigenvalues and eigenvectors and different wavenumbers [15]. This becomes further complicated when there are multiple sensors and channels with possible correlations, which approach is the focus of this chapter. Therefore, we resort to experiments to directly study the correlations between multiple wireless channels in drill strings.

Here, we study multichannel reception using several receivers to improve communication system performance. We propose a strain sensor and a tri-axial accelerometer as a four-channel receiver. Given the complexity of studying the strain

channel and the three acceleration channels analytically, we conduct experiments to obtain these channels' impulse responses. Our measurements show that these wireless channels are nearly uncorrelated and therefore can provide diversity gain. This is further confirmed by the low bit error rates that this system provides. Comparison with single channel receivers shows the benefits of the proposed system for wireless communications via drill strings.

Section 5.1 introduces signals and channels, and the testbed and measurements are presented in Section 5.2. Sections 5.3 and 5.4 discuss measured channel correlations, followed by system performance analysis.

5.1 Definitions of Signals and Channels

Consider an actuator placed on one end of the drill string, which transmits the signal $\gamma(t)$, by converting it from electric form to acoustic waves. At the other end of the drill string we consider two different sensor types that receive propagated acoustic signals and convert them to electric signals. The first sensor is a tri-axial accelerometer which measures local vibrations' accelerations in three orthogonal directions x, y, and z, whereas the second one is a strain sensor that measures the local fractional displacement due to the vibrations. More specifically, let $u_x(t)$, $u_y(t)$, and $u_z(t)$ be the time-varying local displacements due to vibrations at a certain point on a pipe where the accelerometer and strain sensor are mounted (see Figure 5.1, with the two sensors spaced by δ). The acceleration signals are second derivatives of the displacement signals

$$a_i(t) = \partial^2 u_i(t) / \partial t^2, \qquad i = x, y, z.$$

(5.1)

Additionally, the strain signal is the spatial derivative of the displacement signal along the axis of the strain sensor [12]. Since in Figure 5.1 the strain sensor is aligned with the pipe axis, which is in the x direction, we obtain
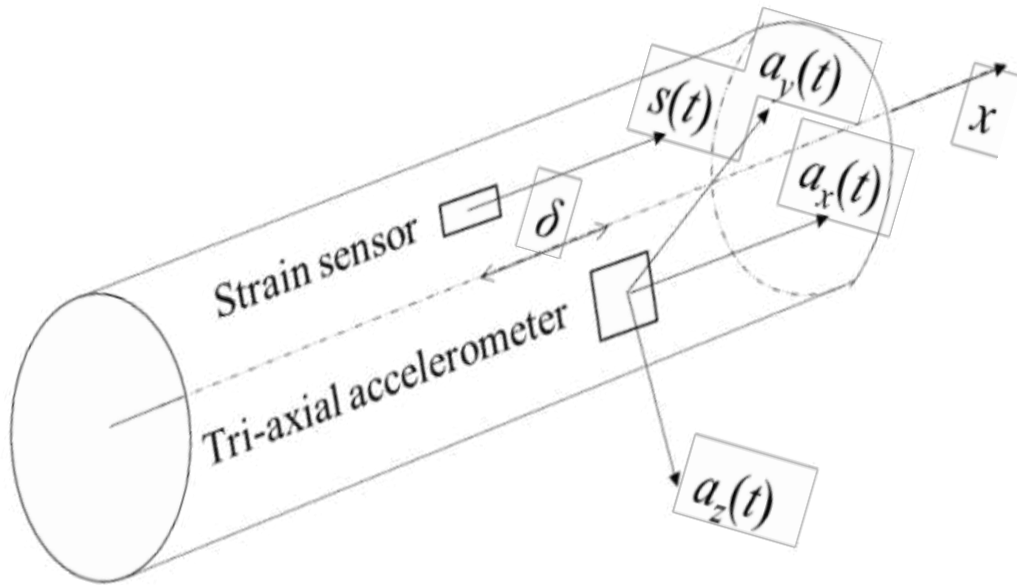
Figure 5.1 Schematic of a tri-axial accelerometer and a strain sensor mounted on a pipe and spaced by δ, serving as the four-channel receiver.

$$s(t) = \partial u_x(t) / \partial x$$

(5.2)

Let the impulse responses of the four-channel receiver be represented by $h_x(t), h_y(t), h_z(t),$ and $h_s(t)$ where the first three are for the tri-axial accelerometer and the last one represents the strain sensor. Upon transmitting the signal $\gamma(t)$, the four received signals can be written as

$$r_i(t) = h_i(t) \oplus \gamma(t) + n_i(t), \quad i = x, y, z, s. \tag{5.3}$$

where $\oplus$ is for convolution and $n_i(t)$ represents noise in the i-th channel. In the next section we show how these four channel impulse responses can be obtained from acceleration and strain measurements of the sensors given in equations (5.1) and (5.2).
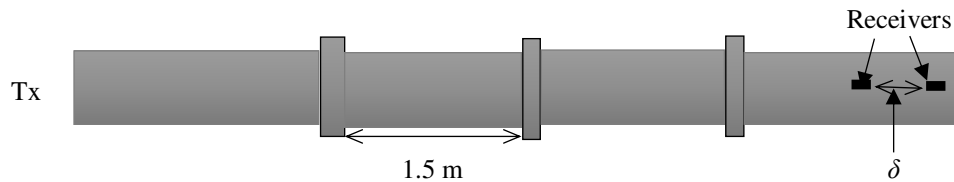
Figure 5.2 The drill string testbed, not drawn to scale. The transmitter Tx is on the left, whereas the two receive sensors are on the right. One receive sensor is fixed at the end of the last pipe, and the other sensor is placed at a variable distance $\delta = 0, 10, 20, 30, 40,$ and 50 cm.

5.2 The Testbed and Channel Measurements

The drill string testbed consists of four steel pipes connected via tool joints (Figure 5.2). The length and diameter of each pipe are 60 and 4 inches, respectively (about 1.5 m and 10 cm, respectively). The length of each tool joint is 3.5 inches (about 9 cm). The transmitter is an actuator (Etrema's model CU18A) that can supply vibrations up to 20 kHz. Since acoustic waves can propagate in a drill string in different modes [12], here we consider two types of excitations, axial and radial, as shown in Figure 5.3a and Figure 5.3b, respectively, to study and compare their channel correlation properties. The receiver includes a tri-axial accelerometer (PCB's model 356B21) and a strain sensor (PCB's model 740B02), as shown in Figure 5.3c.

Channel Estimation Method: To estimate the channel impulse responses sensed by these two sensors, we probe the drill string by a one second linear frequency-modulated chirp signal over the frequency range of 0.4 to 9.2 kHz, with a slope of 8.8 kHz/sec., applied to a power amplifier followed by the actuator. At the receiver side, signals measured by the sensors are sampled at a rate of 40 ksamples/sec using a multichannel analog-to-digital converter and are then fed into a computer. Cross-correlation of the received signals with the chirp signal provides measurements of the channel impulse responses in the drill string [17].

The acceleration and strain signals measured by the sensors are different physical quantities with different units. In such scenarios, when different types of signals are used in a multichannel receiver, they should be converted to the same unit [18].

(a)

(c)

(b)

Figure 5.3 Transmitter and receivers on the drill string: (a) actuator mounted for axial excitation along the drill string axis, (b) actuator mounted for radial excitation perpendicular to the drill string axis, (c) tri-axial accelerometer (right) and strain sensor (left) mounted on the receiver side.

The unit of acceleration is m/sec^2, whereas strain in equation (5.2) is dimensionless. However, since typically its value is much smaller than one, for convenience, it is usually

presented in the dimensionless µε unit, where $1\mu = 10^{-6}$ and ε refers to strain. Additionally, sensor sensitivities are not the same and also have different units: the unit of accelerometer sensitivity β_a is milliV/g, where g = 9.8 m/sec^2 is the gravitational acceleration, whereas the unit of strain sensor sensitivity β_s is milliV/µε. To unify these different units, we find it useful to convert strain to acceleration. Similarly to [12], consider a plane wave for the displacement signal along the pipe axis, i.e., $u_x(t) = \exp(j(\omega t - kx))$, where $j^2 = -1$, ω is the angular frequency and k is the wavenumber. With $k = \omega / V$ in nondispersive media, where V is the wave speed, substitution of $u_x(t)$ into equation (5.2) results in $s(t) = (-j/V)\omega u_x(t)$. Using equation (5.1) we similarly obtain $a_x(t) = -\omega^2 u_x(t)$. Putting these together yields $a_x(t) = -Vj\omega s(t)$. Therefore, a differentiator filter can be used to convert strain to acceleration [12].

Overall, we multiply the readouts of the tri-axial accelerometer, which are in milliV, by the factor g / β_a, which converts the units to m/sec^2. Upon taking the derivative of the readout of the strain sensor, which is in milliV, multiplying it by $-V$, and then by the factor $10^{-6} / \beta_s$ we convert the strain unit to m/sec^2 as well. For sensor sensitivities we have $\beta_a =$ 10 milliV/g per channel and $\beta_s = 50$ milliV/µε. The four channel impulse responses $h_x(t), h_y(t), h_z(t)$ and $h_s(t)$ obtained from the tri-axial accelerometer and strain sensor are shown in Figure 5.4.
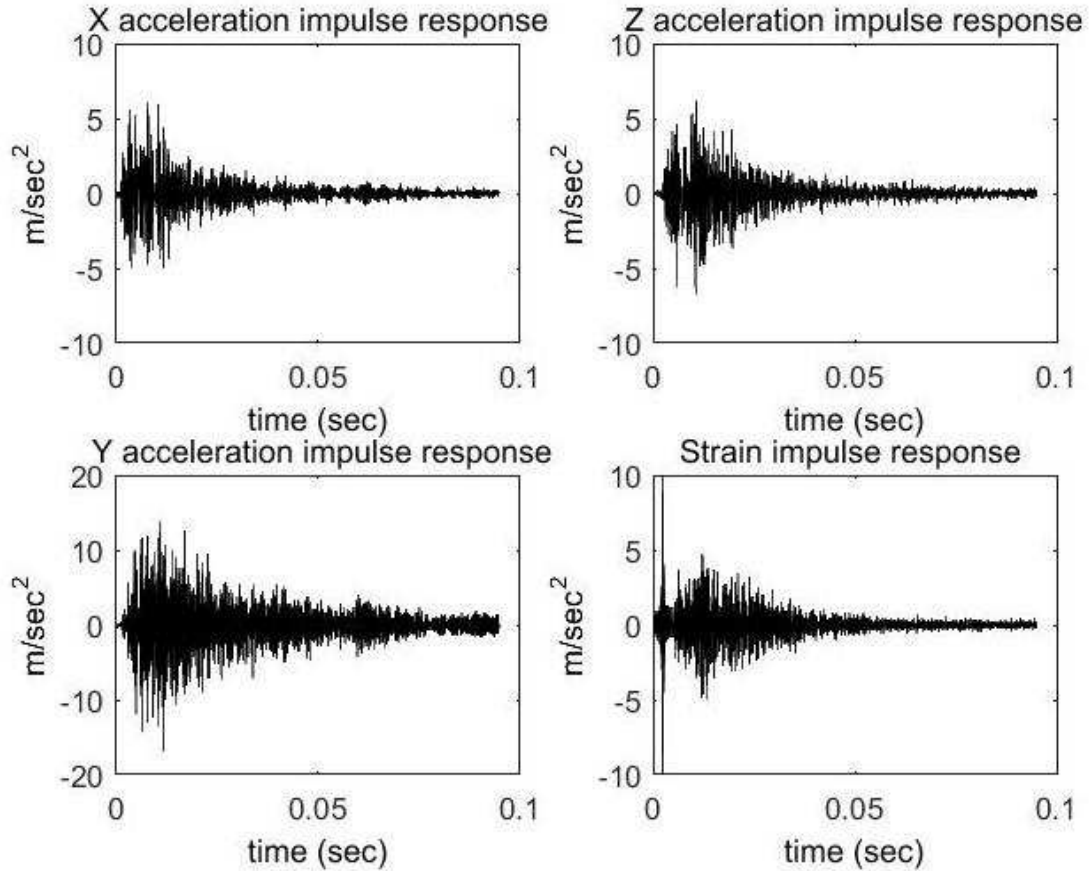
Figure 5.4 Drill string impulse responses of the four-channel receiver measured by the tri-axial accelerometer and the strain sensor.

5.3 Correlations Obtained from Measured Channels

Strain and Acceleration Correlations: In Figure 5.5 measured correlation magnitudes between strain and acceleration channels, after conversion to complex baseband equivalents, are shown for axial excitation as a function of the spacing between the strain sensor and the tri-axial accelerometer. Overall, correlations between the strain and acceleration channels are small, and they decrease as the sensor spacing increases. More importantly, for $\delta = 0$, where the two sensors are next to each other and therefore form a compact multichannel receiver, all correlations between the channels are below 0.3. To

understand the benefit of using the proposed strain sensor and tri-axial accelerometer system, we replace them by two single-channel accelerometers (PCB's model 352C33) and measure their impulse response correlations. As shown in Figure 5.5, for small spacings, single-channel acceleration correlations are much higher than strain/tri-axial correlations. For $\delta = 0$, they show a high average correlation of about 0.75. The impact of such a high correlation is analyzed in the next section.
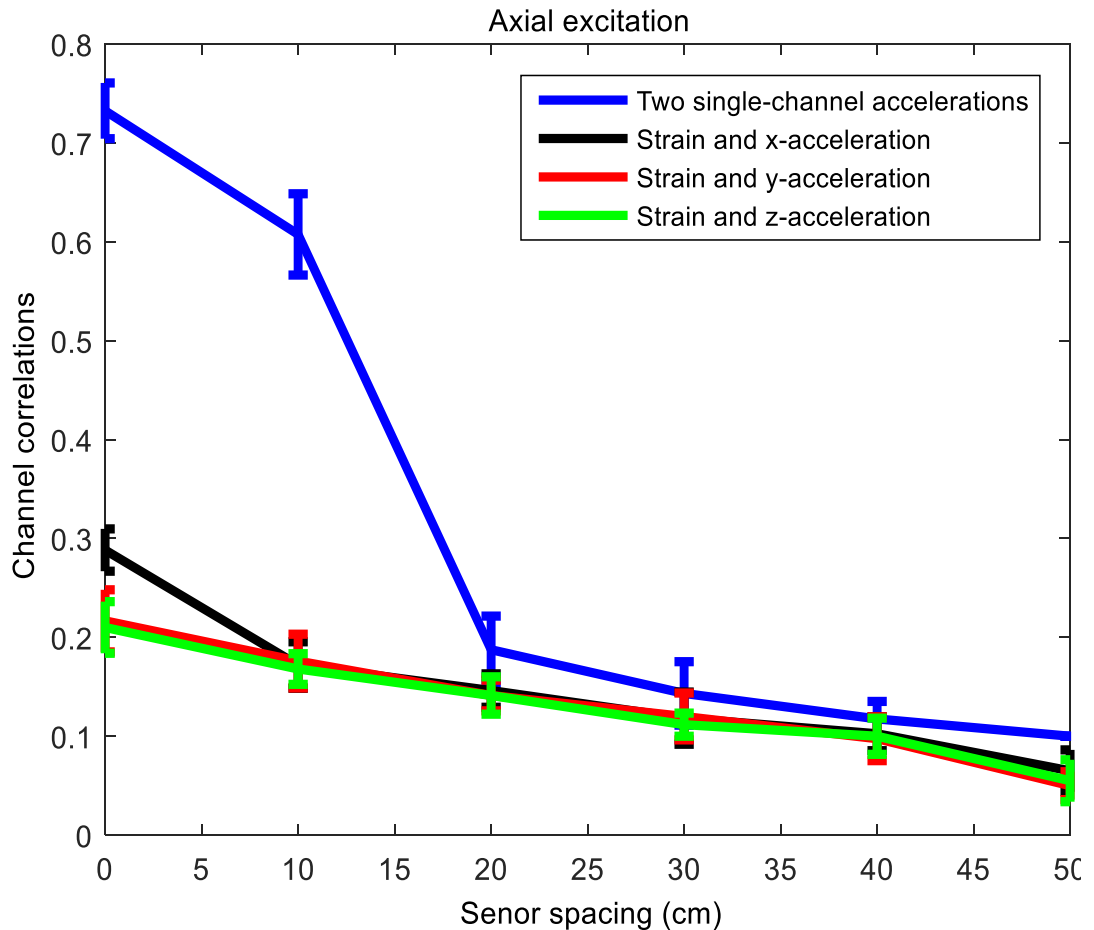
Figure 5.5 Measured correlation magnitudes (means plus/minus standard deviations) between strain and tri-axial acceleration channels versus sensor spacing δ, for axial excitation. As a reference, correlations between two δ-spaced single-channel accelerometers measured under the same setup are shown as well.

Figure 5.6 shows the measured correlation magnitudes between the strain and acceleration channels after conversion to complex baseband equivalents and for radial excitation. We note that for all sensor spacings, correlations remain very low, at less than 0.2. Measured correlations between the impulse responses of two single-channel accelerometers are also shown in Figure 5.6 as a reference. We observe that, for small spacings, single-channel acceleration correlations are much higher than strain/tri-axial correlations. For $\delta = 0$, they show a high correlation of about 0.65. Channel correlation impacts are analyzed in the next section.

Given that the axial data sets of multiple measurements for various spacings in Figure 5.5 show small standard deviations, and since the testbed is time invariant, repeating experiments for Figure 5.6 will provide similar results with small variations. In addition, small changes in receiver correlations typically result in negligible changes in system performance due to the nonlinear relation between receiver correlation and bit error rate [13].

Acceleration Correlations: For axial excitation and six measurement sets over the 0.5 m interval, average correlation magnitudes plus/minus standard deviations in the tri-axial accelerometer for the acceleration channel pairs (x,y), (x,z), and (y,z) are 0.33 +/- 0.04, 0.17 +/- 0.06 and 0.12 +/- 0.03, respectively. For radial excitation, these correlation statistics are 0.12 +/- 0.02, 0.08 +/- 0.03 and 0.1 +/- 0.02, respectively. All of these correlations appear to be small.
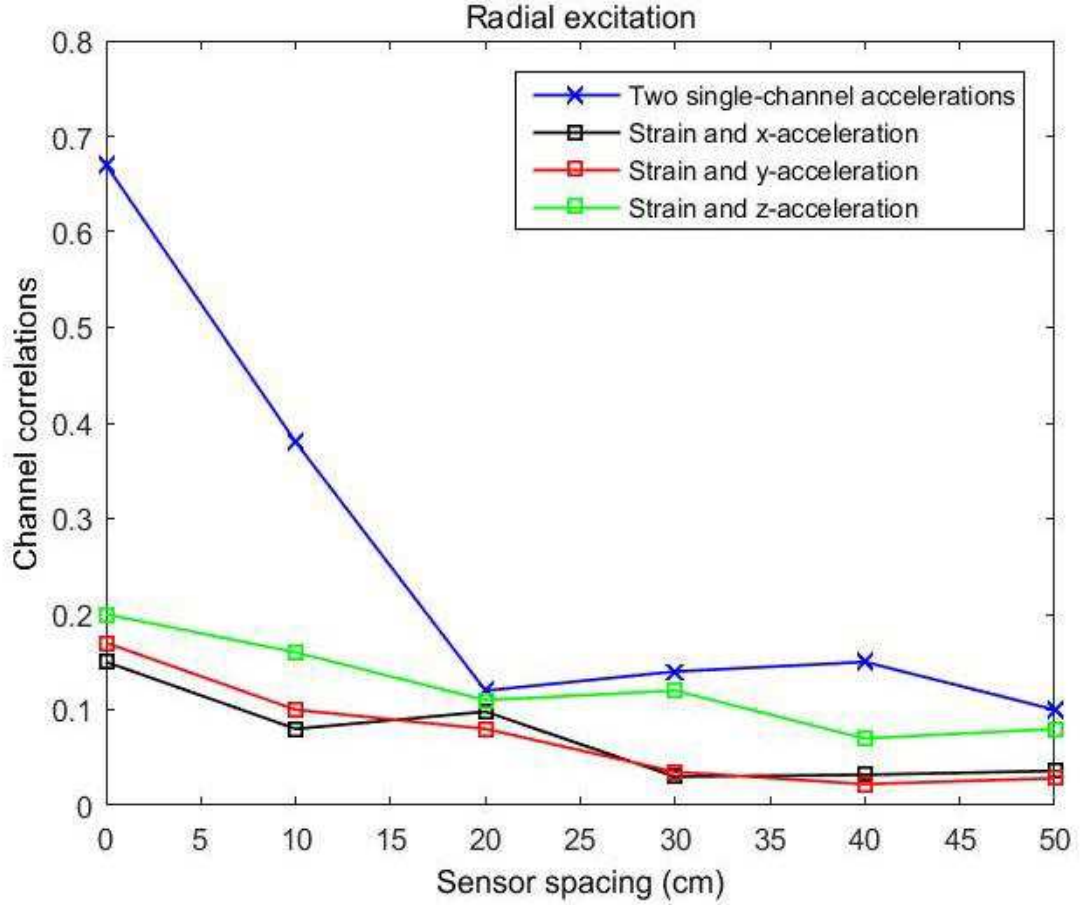
Figure 5.6 Measured correlation magnitudes between strain and tri-axial acceleration channels versus the sensor spacing δ, for radial excitation. As a reference, correlations between two δ-spaced single-channel accelerometers measured under the same setup are shown as well.

5.4 Performance Analysis Using Measured Channels

System Equations: Here we study the performance of the proposed four-channel receiver composed of a tri-axial accelerometer and a strain sensor, as well as the possible impacts of channel correlations. The complex baseband equivalent of equation (5.3) is given by

$\tilde{r}_i(t) = \tilde{h}_i(t) \oplus \tilde{\gamma}(t) + \tilde{n}_i(t), \ \ i = x, y, z, s.$ Using this, the received signals for a block system

model [19] can be written as

$$\mathbf{R} = \mathbf{H}\boldsymbol{\Gamma} + \mathbf{N}, \quad \mathbf{R} = \begin{bmatrix} \mathbf{R}_x \\ \mathbf{R}_y \\ \mathbf{R}_z \\ \mathbf{R}_s \end{bmatrix}, \quad \mathbf{H} = \begin{bmatrix} \mathbf{H}_x \\ \mathbf{H}_y \\ \mathbf{H}_z \\ \mathbf{H}_s \end{bmatrix}, \quad \textbf{and} \quad \mathbf{N} = \begin{bmatrix} \mathbf{N}_x \\ \mathbf{N}_y \\ \mathbf{N}_z \\ \mathbf{N}_s \end{bmatrix}. \tag{5.4}$$

Here $\boldsymbol{\Gamma} = [\tilde{\gamma}_0 \dots \tilde{\gamma}_{K-1}]^T$ is a block of K transmitted symbols and ^{T} stands for transpose. With M the number of channel taps and $i = x, y, z, s$, where $\mathbf{R}_i = [\tilde{r}_i(0) \dots \tilde{r}_i(K + M - 2)]^T$ and $\mathbf{N}_i = [\tilde{n}_i(0) \dots \tilde{n}_i(K + M - 2)]^T$ are the i-th received signal and noise vectors, respectively. Also $\mathbf{H}_i$ is the i-th banded channel convolution matrix whose dimension is $(K + M - 1) \times K$

$$\mathbf{H}_i = \begin{bmatrix} \tilde{h}_i(0) & & \\ \vdots & \ddots & \tilde{h}_i(0) \\ \tilde{h}_i(M-1) & \ddots & \vdots \\ & & \tilde{h}_i(M-1) \end{bmatrix}, \quad i = x, y, z, s. \tag{5.5}$$

The Receiver: With perfect channel knowledge at the receiver, and where elements of equation (5.5) are the measured channels from Section 5.2, the minimum variance unbiased estimate of the vector $\boldsymbol{\Gamma}$ is [17]

$$\hat{\boldsymbol{\Gamma}} = \mathbf{H}^+ \mathbf{R} = \boldsymbol{\Gamma} + \mathbf{H}^+ \mathbf{N}, \quad \mathbf{H}^+ = (\mathbf{H}^H \mathbf{H})^{-1} \mathbf{H}^H \tag{5.6}$$

where $\mathbf{H}^+$ is the pseudo inverse and ^{H} is the transpose conjugate. Covariance of the symbol estimation error vector $\hat{\mathbf{\Gamma}} - \mathbf{\Gamma}$ yields [17]

$$\mathbf{W} = E[(\hat{\mathbf{\Gamma}} - \mathbf{\Gamma})(\hat{\mathbf{\Gamma}} - \mathbf{\Gamma})^H] = \sigma^2(\mathbf{H}^H\mathbf{H})^{-1} \qquad (5.7)$$

where E is the mathematical expectation and σ^2 stands for the power of the additive complex Gaussian noise. To study the performance of the proposed system, consider that K equi-probable binary phase shift keying (BPSK) symbols are transmitted, i.e., $\tilde{\gamma}_\kappa = \pm 1$, $\kappa = 1,...,K$. The average bit error rate (BER) of the receiver in equation (5.6) over K symbols can be written as [19] [20]

$$\bar{P}_e = K^{-1}\sum_{\kappa=1}^{K} Q\left(\sqrt{2/w_{\kappa\kappa}}\right) \qquad (5.8)$$

where $w_{\kappa\kappa}$ is the κ-th diagonal element of $\mathbf{W}$ in equation (5.7) and $Q(\theta) = (2\pi)^{-1/2}\int_\theta^\infty \exp(-\xi^2/2)d\xi.$

BER Results: Figure 5.7 shows the average BER of the four-channel receiver composed of a tri-axial accelerometer and a strain sensor, computed using equations (5.7) and (5.8), and the measured channel impulse responses with axial excitation and $K = 200$. Compared to the average BER of a benchmark system whose receiver is a single-channel accelerometer, also shown in Figure 5.7, the proposed system exhibits a significant performance improvement. To understand the benefit of using the proposed strain sensor

and tri-axial accelerometer system, we replace them by two single-channel accelerometers and compute the average BER of this system using equations (5.7) and (5.8), where $\mathbf{H} = [\mathbf{H}_1^T \; \mathbf{H}_2^T]^T$ contains banded channel convolution matrices measured by the two single-channel accelerometers. As shown in Figure 5.7, this average BER is approximately the same as the average BER of the benchmark system whose receiver is a single-channel accelerometer. This nearly similar BER can be attributed to the high correlation between the two single-channel accelerometers, i.e., 0.75, as discussed in the previous section. This implies almost no diversity gain. On the other hand, all correlations between all channels of the strain/tri-axial receiver are small, at below 0.33, according to the previous section. This indicates a high diversity gain that can explain the low BER in Figure 5.7.

Channel Estimation Error: In practice, the assumed perfect channel knowledge is not available and the channel should be estimated at the receiver. The estimated channel matrix can be written as $\hat{\mathbf{H}} = \mathbf{H} + \eta\mathbf{E}$ [21], where $\mathbf{E}$ is estimation error matrix whose non-zero elements are unit-variance complex Gaussians, and η specifies channel estimation accuracy ($\eta = 0$ means perfect channel estimate). The resulting symbol vector estimate is $\hat{\mathbf{\Gamma}} = \hat{\mathbf{H}}^+\mathbf{R}$. For fairly accurate channel estimates, $\eta \ll 1$, we similarly to [21] use a Taylor expansion $\hat{\mathbf{H}}^+ = (\mathbf{H} + \eta\mathbf{E})^+ \approx \mathbf{H}^+ - \eta\mathbf{H}^+\mathbf{E}\mathbf{H}^+$, which results in $\hat{\mathbf{\Gamma}} \approx \mathbf{\Gamma} + \mathbf{H}^+\mathbf{N} - \eta\mathbf{H}^+\mathbf{E}\mathbf{\Gamma} - \eta\mathbf{H}^+\mathbf{E}\mathbf{H}^+\mathbf{N}$. Comparing with equation (5.6), we observe that imperfect channel knowledge, $\eta \neq 0$, introduces additional noise-like terms. To see how this affects the system performance, the average BER of the four-channel receiver is shown in Figure 5.7 for $\eta = 0.05, 0.1, 0.15$, which measurements are obtained by perturbing the measured channels in $\mathbf{H}$ via $\hat{\mathbf{H}} = \mathbf{H} + \eta\mathbf{E}$, and then counting the number of differences

between the transmitted symbol vector $\boldsymbol{\Gamma}$ and its estimate $\hat{\boldsymbol{\Gamma}}$. We observe that imperfect channel knowledge causes some performance loss. For example, for BER of 0.02 and $\eta = 0.15$, there is a 3 dB Signal-to-Noise Ratio (SNR)loss in Figure 5.7.
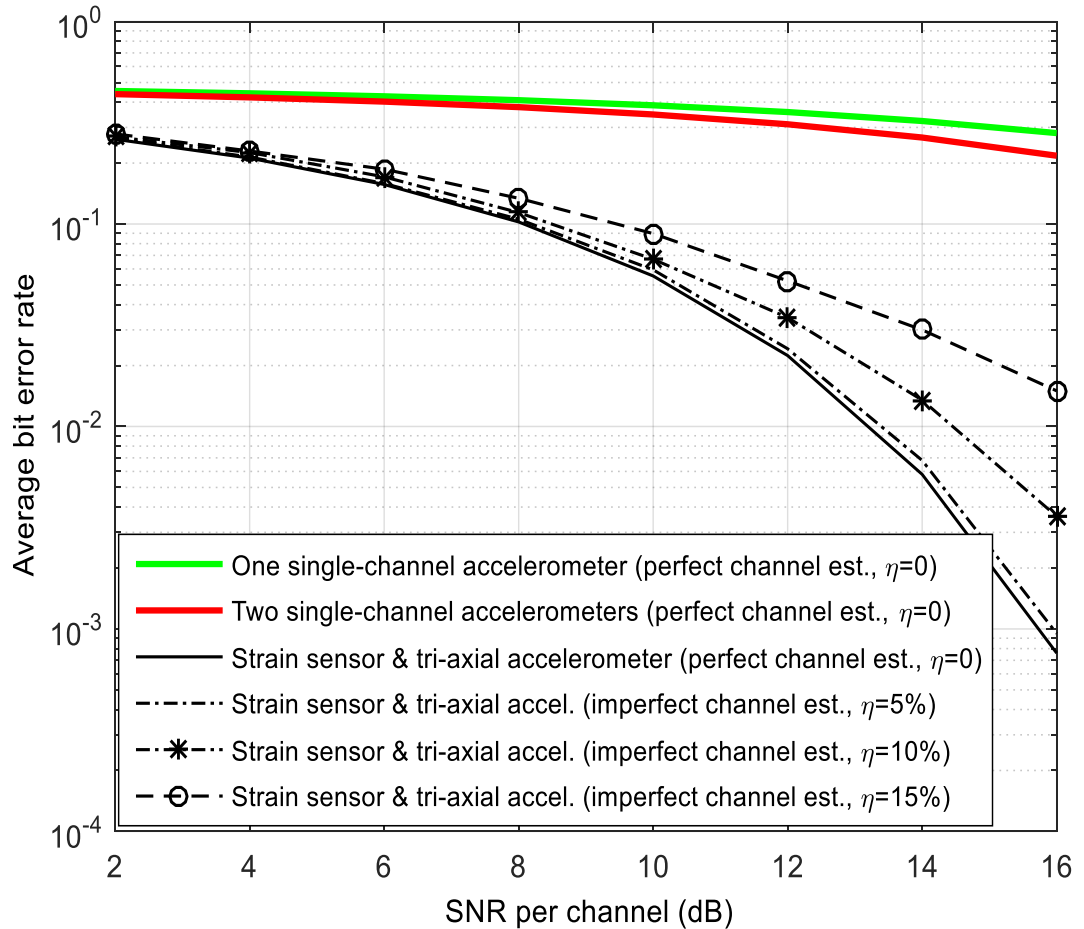

Figure 5.7 Average bit error rate of three different receivers on the drill string: one single-channel accelerometer (green), two single-channel accelerometers (red), and a strain sensor together with a tri-axial accelerometer (black).

CHAPTER 6

CONCLUSION

In this dissertation, we investigate the use of a strain receiver and a multi-channel receiver in application to acoustic borehole communication based on experimental results. Transmission of information about the circumstances around the drill bit is critical in oil well drilling operation. The commercial telemetry used today in borehole communication during the drilling of oil wells is the mud-pulse method. This method makes use of the mud that is used to carry formation cuttings from downhole to surface to sends information using a valve that controls the mud flow rate. However, this method can provide only a low data transmission rate that for a typical situation is less than 10 bits per second. Acoustic communication is a promising method for borehole communication, where the acoustic waves propagate through the drill string. The main problem of this method is the huge reflections due to the mismatch between the pipes and tool joints.

Two types of receivers for communication via drill strings in oil wells are studied. The first one is a tri-axial multichannel accelerometer which measures acceleration signals in three orthogonal dimensions, whereas the second is composed of two single channel accelerometers. Analysis of the measured channel impulse responses collected from our drill string testbed, and presented in this dissertation, reveals that the tri-axial acceleration channels are nearly uncorrelated, whereas the single channel accelerometers are highly correlated. This indicates that the tri-axial receiver is capable of providing diversity gain and therefore better performance by relying on its orthogonal channels. This is further demonstrated in the dissertation by looking at the multichannel eigen spectrum, which

shows the value of the tri-axial receiver.

We also investigate the performance of a strain receiver and compare this with an accelerometer receiver. The strain channel shows better performance in terms of normalized eigenvalue compared with the acceleration channel for use in borehole communication systems. In addition, the strain channel also has superior performance in term of bit error when compared to the acceleration channel. In terms of channel characteristics, the delay spread of the strain channel is almost half the delay spread of the acceleration channel.

A multichannel receiver for wireless communication through drill strings is introduced. The channels in the system are strain together with three acceleration channels. Using measured channel impulse responses, it is shown that these channels are nearly uncorrelated, so that the multichannel receiver can provide diversity gain. This is demonstrated by a system performance analysis, which shows small bit error rates compared to single-channel receivers or receivers with highly correlated channels.

REFERENCES

[1]   O. Kotlyar. Universal mud pulse telemetry system. U. S. Patent No.4771408, 1987.

[2]   M. S. Beattie and A. H. Abdallah. Mud pulse telemetry. U. S. Patent No. 6421298, 1999.

[3]   N. C. Macleod. Apparatus and method for down-hole EM telemetry while drilling. U. S. Patent No. 4739325, 1986.

[4]   P. F. Rodney. Low frequency electromagnetic telemetry system employing high cardinality phase shift keying. U. S. Patent No. 6750783, 2002.

[5]   W. H. Cox and P. E. Chaney. Telemetry systems. U. S. Patent No. 4,293,936, 1981.

[6]   T. G. Barnes and B. T. Kirkwood, "Passbands for acoustic transmission in an idealized drill string", *The Journal of the Acoustical Society of America*, 51:1606-1608, 1972.

[7]   D. S. Drumheller, "Acoustical properties of drill strings", *The Journal of the Acoustical Society of America*, 85(3):1048-1064, March 1989.

[8]   N. J. C. Lous, S. W. Rienstra, and I. B. F. Adan, "Sound transmission through a periodic cascade with application to drill pipes", *The Journal of the Acoustical Society of America*, 103(5):2302-2311, May 1998.

[9]   M. Memarzadeh, Optimal Borehole Communication Using Multicarrier Modulation, PhD thesis, Rice University, Huston, Texas, USA, January 2007.

[10]   S. Sinanovic, D. H. Johnson, and W. R. Gardner, "Directional propagation cancellation for acoustic communication along the drill string", *Proceedings-IEEE International Conference on Acoustics Speech and Signal Processing,* vol. v4, pp. 521-524, 2006.

[11]   J. F. Claerbout, *Fundamentals of geophysical data processing: with applications to petroleum prospecting*. Blackwell Scientific Publications, 1985.

[12]   F. Poletto, , M. Malusa, , F. Miranda, & U. Tinivella, (2004). Seismic-while-drilling by using dual sensors in drill strings. *Geophysics, 69*(5), 1261-1271. doi:10.1190/1.1801943.

[13]   M. K. Simon and M.-S. Alouini, *Digital Communication over Fading Channels*, 2nd ed., Hoboken, NJ: Wiley, 2005.

[14] A. Abdi and H. Guo, "Signal correlation modeling in acoustic vector sensor arrays," *IEEE Trans. Signal Processing*, vol. 57, pp. 892-903, 2009.

[15] M.-S. Alouini and M. K. Simon, "Multichannel reception of digital signals over correlated Nakagami fading channels," in *Proc. 36th Allerton Conf. Commun., Control, and Comput.*, 1998, pp. 146-155.

[16] A. Abdi, H. Guo and P. Sutthiwan, "A new vector sensor receiver for underwater acoustic communication," in *Proc. Marine Technology Society/IEEE Oceans*, 2007, pp. 1-10.

[17] S. M. Kay, *Fundamentals of Statistical Signal Processing: Estimation Theory*. Englewood Cliffs, NJ: PTR Prentice-Hall, 1993.

[18] A. Abdi and H. Guo, "A new compact multichannel receiver for underwater wireless communication networks," *IEEE Trans. Wireless Commun.*, vol. 8, pp. 3326-3329, 2009.

[19] C. Tepedelenlioglu and Q. Ma, "On the performance of linear equalizers for block transmission systems," in *Proc. IEEE Global Telecommun. Conf.*, St. Louis, MO, 2005, pp. 3892-3896.

[20] C. Chen and A. Abdi, "Signal transmission using underwater acoustic vector transducers," *IEEE Trans. Signal Processing*, vol. 61, pp. 3683-3698, 2013.

[21] C. Wang, E. K. S. Au, R. D. Murch, W. H. Mow, R. S. Cheng and V. Lau, "On the performance of the MIMO zero-forcing receiver in the presence of channel estimation error," *IEEE Trans. Wireless Commun.*, vol. 6, pp. 805-810, 2007.

[22]   A. K. Farraj, S. L. Miller and K. A. Qaraqe, "Channel characterization for acoustic downhole communication systems," in *Proc. SPE Annual Technical Conference and Exhibition*, 2012, pp. 1–12.

[23] M. A. Gutierrez-Estevez, U. Krueger, K. A. Krueger, K. Manolakis and V. Jungnickel, "Acoustic channel model for adaptive downhole communication over deep drill strings," in *Proc. IEEE Int. Conf. Acoustics, Speech and Signal Processing*, 2013, pp.4883-4887.

 [24]   F. B. Poletto and F. Miranda, *Seismic While Drilling: Fundamentals of Drill-Bit Seismic for Exploration*. Boston: Elsevier, 2004.

[25] T. S. Rappaport, *Wireless Communications: Principles and Practice*, 2nd ed., Upper Saddle River, NJ: Prentice Hall PTR, 2002.